Quasiperiodicity, band topology, and moiré graphene

Dan Mao and T. Senthil
Department of Physics, Massachusetts Institute of Technology, Cambridge, Massachusetts 02139, USA

(Received 7 December 2020; accepted 24 February 2021; published 4 March 2021)

A number of moiré graphene systems have nearly flat topological bands where electron motion is strongly correlated. Though microscopically these systems are only quasiperiodic, they can typically be treated as translation invariant to an excellent approximation. Here we reconsider this question for magic angle twisted bilayer graphene that is nearly aligned with a hexagonal boron nitride (hBN) substrate. We carefully study the effect of the periodic potential induced by hBN on the low energy physics. The combination of this potential and the moiré lattice produced by the twisted graphene generates a quasiperiodic term that depends on the alignment angle between hBN and the moiré graphene. We find that the alignment angle has a significant impact on both the band gap near charge neutrality and the behavior of electrical transport. We also introduce and study toy models to illustrate how a quasiperiodic potential can give rise to localization and change in transport properties of topological bands.

DOI: 10.1103/PhysRevB.103.115110

I. INTRODUCTION

Following the discovery of correlated insulators and superconductivity in magic angle twisted bilayer graphene (MATBG) in 2018 [1,2] a tremendous amount of attention has been lavished on moiré materials. Other moiré systems displaying correlated electron physics include ABC trilayer graphene (TLG/hBN) nearly aligned with a hexagonal boron-nitride (hBN) substrate [3], twisted double bilayer graphene [4], twisted monolayer-bilayer graphene [5], and twisted transition metal dichalcogenides [6]. Our interest in this paper is on MATBG that is further nearly aligned with a hBN substrate (MATBG/hBN) [7,8] which alters the observed phenomena.

In MATBG/hBN Ref. [7] discovered ferromagnetism and an associated large anomalous Hall effect at 3/4 filling of the conduction band. Subsequently Ref. [8] studied devices of MATBG/hBN which not only showed emergent ferromagnetism at 3/4 conduction band filling but also observed a quantized anomalous Hall effect with $\sigma_{xy} = \frac{e^2}{h}$. Theoretically the near alignment with the hBN breaks the C_2 symmetry of 180 degree rotation within the graphene plane and opens up a gap between the valence and conduction bands which—in the absence of alignment—touch at Dirac points. The resulting bands within a single valley were found [9,10] to have Chern number ± 1 (with opposite valleys having opposite Chern number). As discussed in Ref. [11] such nearly flat $\pm$ Chern bands are, in fact, common to a number of moiré graphene materials. Upon including electron-electron interactions, Ref. [11] also proposed these systems to be excellent platforms to show a quantum anomalous Hall effect at total (i.e., including spin and valley) odd integer filling. These ideas were developed further in the specific context [9,10] of MATBG/hBN and in ABC TLG/hBN which too displays emergent ferromagnetism and a quantum anomalous Hall effect [3].

In this paper we revisit the theory of single particle states of MATBG/hBN. The presence of hBN layer has two effects on the nearby graphene. One is that hBN induces a constant sublattice potential difference, which is studied in detail in Refs. [9,10]. The other is that it induces a second periodic moiré potential which may or may not be commensurate with the original moiré potential of the TBLG system, which is considered in recent studies [12–14]. The previous theoretical work [9,10] ignored the moiré potential introduced by the near alignment with the hBN, mostly for simplicity but also on the grounds that its estimated strength is smaller than the TBLG moiré potential. In the present paper we go beyond this approximation and carefully include both moiré potentials. We first determine the conditions—which we dub "perfect alignment"—under which the two moiré potentials are commensurate. This concept of perfect alignment is distinct from the naive expectation that the perfect situation is when the twist angle between one graphene layer and hBN is zero. When the perfect alignment condition is satisfied, translation invariance is preserved and we can define a crystal momentum and a (reduced) Brillouin zone. Away from perfect alignment, the two moiré potentials are incommensurate, and translational symmetry is completely broken [15]. The low energy physics can be modeled by introducing a quasiperiodic potential to topological bands (in the case of TBLG/hBN, Chern bands with opposite Chern numbers).

Electronic systems with a quasiperiodic potential (QP) have been studied extensively in 1D. (See Ref. [16] for a detailed review.) In the 1D Audry-André model, there is a localization transition with the increase of quasiperiodic potential strength [17]. In higher than 1D, an intermediate phase with eigenstates delocalized in both real space and momentum space can exist between an extended phase and a localized phase [18]. The generic existence of such an intermediate phase in a 2D system with quasiperiodic potential has not been

settled yet, but it is not our focus in this paper. There also have been studies of semimetals subjected to QP, where interesting semimetal-to-metal phase transition and subdiffusive transport are found [19–21]. Here we are particularly interested in the effect of a quasiperiodic potential on topological bands [22]. In momentum space, a nonvanishing Chern number can impose nontrivial phase structure on the wave function, which may change the localization properties when a quasiperiodic potential is added to the system compared to trivial bands.

In the case of perfect alignment, there is a clean separation between valence and conduction bands. Then if—due to interactions—the system is valley and spin polarized at total odd integer filling ν_T, electrons will completely fill a Chern band, and there will be a quantum anomalous Hall effect. Away from perfect alignment, the quasiperiodic potential induces in-gap states—which are not real-space localized—between the valence and conduction bands. Then we show by explicit calculation that even with full valley and spin polarization at odd integer ν_T, there is no quantization of the anomalous Hall conductivity. Thus observation of a quantum anomalous Hall effect at such fillings is aided by studying devices that are tuned close to perfect alignment. We show, however, that strain can be used to tune the alignment condition, thereby enabling engineering flat well-separated Chern bands in TBLG/hBN devices.

Though we do not address many body effects in this paper, we note that the presence of in-gap states is likely to hinder the development of valley/spin polarization in the first place. This is because they can roughly be thought of as increasing the bandwidth of the active valence or conduction band, thereby reducing the ability of interactions to induce ferromagnetism. Thus it is desirable to stay close to perfect alignment. Indeed the two devices studied in Refs. [7,8] are nearly perfectly aligned. This condition may be a more stringent requirement for the fractional quantum anomalous Hall states proposed [23–25] for TBLG/hBN.

The periodic modulation induced by the hBN layer is relevant only if the hBN layer is nearly aligned with TBLG since the moiré lattice constants of the superlattices generated by hBN and TBLG are of the same order as the moiré lattice constant of TBLG. For hBN misaligned with TBLG, due to the lattice mismatch, there is no longer any periodic moiré potential induced by hBN so the QP physics are irrelevant in those systems.

In recent years, Anderson localization and many-body localization in the presence of QP have been investigated in cold atom experiments [26–29]. The interplay between quasiperiodicity and interaction near critical points in quantum Ising and related spin models has been the subject of several studies: see, e.g., Refs. [30–35] for some representative papers. It is seen that the presence of QP can lead to new interacting critical phases which are different from that found with quenched disorder [35]. The specific moiré graphene system we study here provides an experimental context where strongly interacting quantum phases/phase transitions in the presence of quasiperiodicity may be explored.

The rest of the paper is organized as follows. In Sec. II, we explain how the alignment to hBN induces another moiré pattern on top of the original moiré pattern of TBLG system.

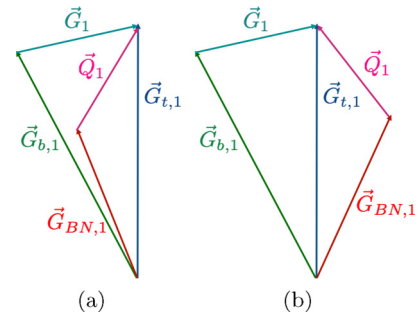

FIG. 1. (a) Case 1, $\theta_{\rm BN} > 0$ and $\theta_G > 0$. (b) Case 2, $\theta_{\rm BN} < 0$ and $\theta_G > 0$. The angles are exaggerated for illustration purpose.

We further study two scenarios in Sec. III and in Sec. IV. One is that the two moiré patterns overlap and the other is that they are incommensurate. In Sec. V, we propose a toy model to address the question of the effect of a quasiperiodic potential on a topological band.

II. TWO MOIRÉ PATTERNS IN hBN/TBLG SYSTEM

Let us consider TBLG with the top graphene layer nearly aligned with hBN. There are two moiré patterns, one formed by the TBLG, the other formed by the top graphene layer and hBN layer. The difference between the two moiré reciprocal lattice vectors is in general not small compared to the reciprocal vectors themselves. Thus, strictly speaking, it is not a valid approximation to define a mini BZ. Let us first write down the reciprocal vectors explicitly. The reciprocal lattice vectors of the top graphene sheet are $\vec{G}_{t,1} = \frac{4\pi}{\sqrt{3}a_G}(0, 1)$ and $\vec{G}_{t,2} = R_{2\pi/3}\vec{G}_{t,1}$, where a_G is the lattice constant of graphene and $R_{2\pi/3}$ denotes counterclockwise rotation by $2\pi/3$. Assuming the bottom graphene layer rotates counterclockwise by an angle $\theta_G \ll 1$, that gives $\vec{G}_{b,1} = R_{\theta_G}\vec{G}_{t,1}$. The TBLG moiré pattern is determined by the two reciprocal lattice vectors, $\vec{G}_1 = \vec{G}_{t,1} - \vec{G}_{b,1} = \frac{4\pi}{\sqrt{3}a_G}(\sin\theta_G, 1 - \cos\theta_G)$ and $\vec{G}_2 = R_{2\pi/3}\vec{G}_1$. Now adding hBN on top, assuming the hBN layer rotates by an angle $\theta_{\rm BN} \ll 1$ with respect to the top layer of TBLG, there is a second moiré pattern, which is generated by the lattice mismatch of the hBN layer and the top graphene layer. For the reciprocal lattice vectors for this second moiré pattern, we write $\vec{Q}_1 = \vec{G}_{t,1} - \vec{G}_{BN,1} = (\frac{4\pi}{\sqrt{3}a_{\rm BN}}\sin\theta_{\rm BN}, \frac{4\pi}{\sqrt{3}a_{\rm BN}}\cos\theta_{\rm BN} - \frac{4\pi}{\sqrt{3}a_G})$, $\vec{Q}_2 = R_{2\pi/3}\vec{Q}_1$, where $a_{\rm BN}$ is the lattice constant of hBN.

For the special combination of $\theta_{\rm BN}$ and θ_G, the two moiré patterns can be commensurate. For simplicity, we only consider the case where these two patterns overlap, which we call "perfect" alignment. This means that the lattice generated by $\vec{G}_{1,2}$ is the same as the lattice generated by $\vec{Q}_{1,2}$, which can be satisfied as long as $|\vec{G}_1| = |\vec{Q}_1|$, and the angle between $\vec{Q}_1$ and $\vec{G}_1$ is $n\pi/3$, where n is an integer. These two conditions can be satisfied when either θ_G and $\theta_{\rm BN}$ have the same sign or have the opposite sign. See Fig. 1 for illustration.

For case 1, $\theta_{\rm BN} > 0$ and $\theta_G > 0$. The angle between $\vec{G}_1$ and $\vec{Q}_1$ is $\pi/3$. For case 2, $\theta_{\rm BN} < 0$ and $\theta_G > 0$. The angle between $\vec{G}_1$ and $\vec{Q}_1$ is $2\pi/3$. We only consider $a_{\rm BN} > a_G$. Using the law

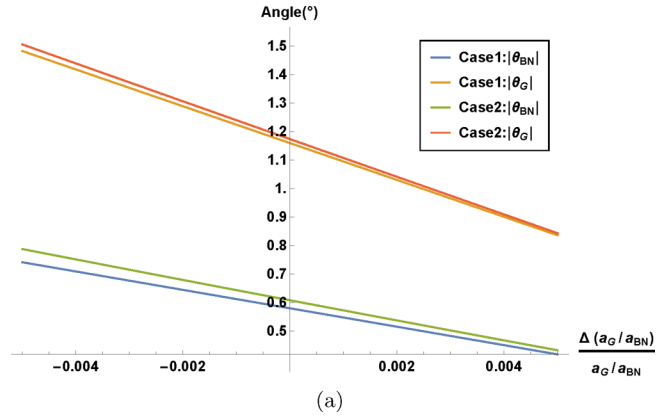

(a)

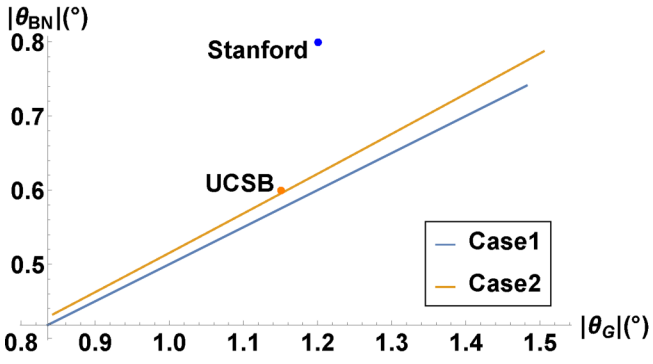

(b)

FIG. 2. (a) Dependence of $|\theta_{\rm BN}|$ and $|\theta_G|$ on the change of the ratio $a_G/a_{\rm BN}$ for satisfying perfect alignment conditions. $\Delta(a_G/a_{\rm BN})$ denotes the change of $a_G/a_{\rm BN}$ from $a_G/a_{\rm BN} = 2.46/2.504$. (b) The points on blue and orange lines are $|\theta_{\rm BN}|$ and $|\theta_G|$ taken from (a). The blue and orange dots are data from two experimental samples from the Stanford group [7] and the UCSB group [8].

of sines one can get

$$\cot|\theta_{\rm BN}| = \left(2\sin\left(\frac{\theta_G}{2}\right)\sin\left(\mp\frac{\theta_G}{2}+\frac{\pi}{6}\right)\right)^{-1} - \cot\left(\mp\frac{\theta_G}{2}+\frac{\pi}{6}\right)$$

$$\frac{a_G}{a_{\rm BN}} = \frac{2\sin\left(\frac{\theta_G}{2}\right)\sin\left(\mp\frac{\theta_G}{2}+\frac{\pi}{6}\right)}{\sin|\theta_{\rm BN}|}, \tag{1}$$

where we take "−" for case 1 and "+" for case 2.

From the perfect alignment conditions Eq. (1), there are two free parameters in a_G, $a_{\rm BN}$, θ_G, and $\theta_{\rm BN}$. If one fixes $a_{\rm BN}$ to be 2.504 Å and a_G to be 2.46 Å, the corresponding $\theta_{G,\rm BN}$ are $\theta_G \approx 1.16^\circ, \theta_{\rm BN} \approx 0.58^\circ$ for case 1 and $\theta_G \approx 1.17^\circ, \theta_{\rm BN} \approx -0.61^\circ$ for case 2. If the graphene sheets are under strain, a_G can be slightly changed. From Fig. 2, we find that $\theta_{\rm BN}$ and θ_G are highly sensitive to the lattice constants and θ_G can be tuned to magic angle with 0.2% changed to $a_G/a_{\rm BN}$. We also plot the experimental value of θ_G and $\theta_{\rm BN}$ [7,8] in Fig. 2(b) and compare them to the perfect alignment case. Note that the sample studied in Ref. [8] is closer to the perfect alignment. This provides an explanation to the better quantization of Hall conductivity in Ref. [8] than in Ref. [7]. Next, we continue to discuss the two kinds of perfect alignments in details in Sec. III.

III. PERFECT ALIGNMENT

As an idealized limit, in this section, we consider perfect alignment between hBN and TBLG. We can still define a mini Brillouin zone, and momentum is a good quantum number in this limit. In the previous experiments [7,8], the TBLG is sandwiched between two hBN layers and only one hBN layer is closely aligned with the TBLG, assuming it is the top layer of the two hBN layers for simplicity. Thus, to make contact with the setups in these experiments, we ignore the hopping between the hBN layer and the bottom layer of the TBLG system in the rest of our discussion. Hopping between the hBN and top layer of TBLG induces two kinds of terms in momentum space of the graphene. One is hopping terms between $\vec{k}$ and $\vec{k}+\vec{Q}_i$'s, where $\vec{Q}_i$'s are the reciprocal vectors of the moiré pattern generated by the hBN and top graphene layer. The other one is a constant AB sublattice potential due to the lattice relaxation in hBN and in graphene and electron-electron interaction (if the lattice is rigid, the sublattice potential vanishes due to the lattice mismatch between hBN and graphene) [36]. In momentum space, the Hamiltonian of the hBN and TBLG system for one valley and one spin can be written as

$$H = H_{\rm TBLG} + H_V, \tag{2}$$

where H_V contains two terms,

$$H_V = \sum_{\vec{k}} f^\dagger_{\vec{k}} m_z \sigma_z f_{\vec{k}} + \sum_{\vec{k},i} (f^\dagger_{\vec{k}} V(\vec{Q}_i) f_{\vec{k}+\vec{Q}_i} + \text{H.c.}), \tag{3}$$

where $f_{\vec{k}} = (f_{\vec{k},A}, f_{\vec{k},B})^T$ denotes the electron annihilation operators for sublattice A and B. σ_z acts on sublattice degrees of freedom. Index $i = 1, \ldots, 6$ labels different reciprocal vectors. $\vec{Q}_1$ is defined in Sec. II and all the other $\vec{Q}_i$'s are generated by performing $\mathcal{C}_6$ rotation of $\vec{Q}_1$ consecutively.

$V(\vec{Q}_i)$'s can be parametrized in the following way [37],

$$V(\vec{Q}_i) = \begin{pmatrix} H_0(\vec{Q}_i) + H_z(\vec{Q}_i) & H_{AB}(\vec{Q}_i) \\ H_{BA}(\vec{Q}_i) & H_0(\vec{Q}_i) - H_z(\vec{Q}_i) \end{pmatrix}, \tag{4}$$

where $H_{0,z}(\vec{Q}_1) = H_{0,z}(\vec{Q}_3) = H_{0,z}(\vec{Q}_5) = C_{0,z}e^{i\phi_{0,z}}$, $H_{0,z}(\vec{Q}_2) = H_{0,z}(\vec{Q}_4) = H_{0,z}(\vec{Q}_6) = C_{0,z}e^{-i\phi_{0,z}}$ and $H_{AB}(\vec{Q}_1) = H^*_{AB}(\vec{Q}_4) = C_{AB}e^{i(\frac{2\pi}{3}-\phi_{AB})}$, $H_{AB}(\vec{Q}_3) = H^*_{AB}(\vec{Q}_2) = C_{AB}e^{-i\phi_{AB}}$, $H_{AB}(\vec{Q}_5) = H^*_{AB}(\vec{Q}_6) = C_{AB}e^{i(-\frac{2\pi}{3}-\phi_{AB})}$. $H_{BA}(\vec{Q}) = H^*_{AB}(-\vec{Q})$ from Hermiticity.

From *ab initio* study [37], at $\theta_{\rm BN} = 0^\circ$, taking the lattice relaxation into account, the parameters for the periodic terms are $C_0 = -9.07$, $\phi_0 = 97.99^\circ$, $C_z = -5.64$, $\phi_z = -3.66^\circ$, $C_{AB} = 7.34$, $\phi_{AB} = 24.53^\circ$. All C's are in units of meV. We take $m_z = 15$ meV in the numerics. In our cases, $\theta_{\rm BN}$ is not always zero, but we adopt the above set of parameters, assuming that the slight change will not alter the low energy physics. Compared to the pure TBLG system, the alignment of hBN layer can in principle open up a gap at K_M points in the mini BZ due to the breaking of $C_2\mathcal{T}$ symmetry induced by hBN [38–40].

We plot the dispersion relation of the valence and conduction bands near charge neutrality at $\theta_G = 1.2^\circ$ in Fig. 3

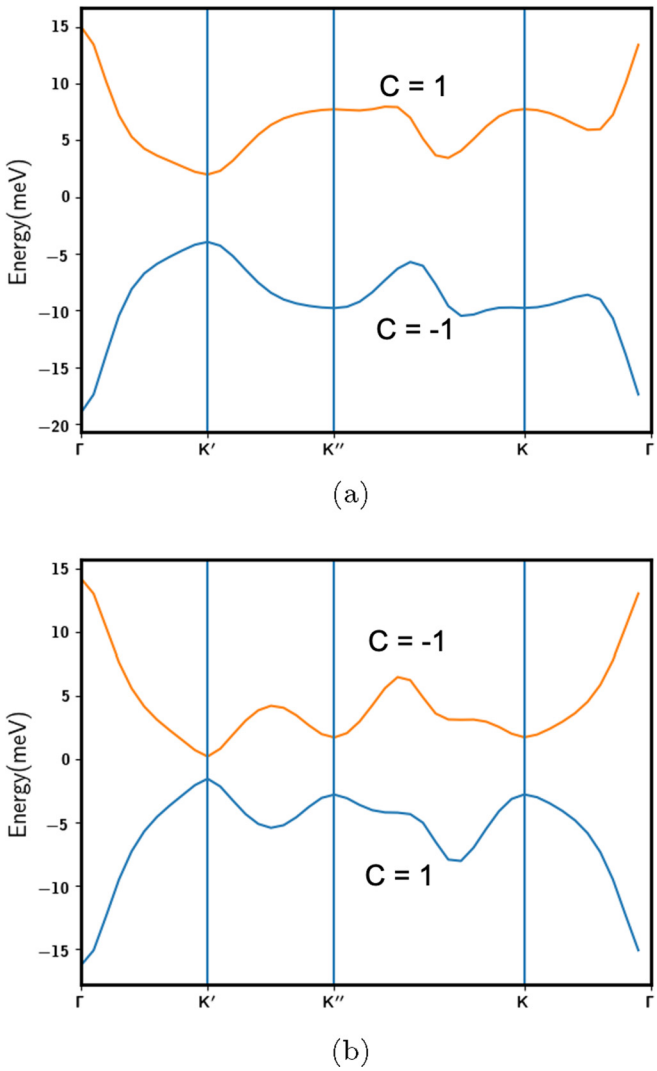

FIG. 3. Dispersion for (a) Case 1 and (b) Case 2. $\theta_G = 1.2^\circ$.

along a path in the mini BZ for both case 1 and case 2. The contribution to the gap of the momentum dependent terms $V(\vec{Q}_i)$'s depends strongly on how hBN is aligned with TBLG. Further calculation shows that in case 1, the two bands near charge neutrality have Chern number ± 1, while in case 2, the Chern numbers get reversed. The distribution of Berry curvature of valence band for various cases is plotted in Fig. 4. For $\theta_G = 1.15^\circ$, we get the same Chern numbers for case 1 and case 2. The distribution of Berry curvature is also similar to $\theta_G = 1.2^\circ$ (see Appendix A). From the numerical calculation, we demonstrate that the alignment with hBN has a significant effect on the low energy physics of the TBLG system. In particular, the periodic potential induced by hBN cannot be ignored.

IV. INCOMMENSURATE ALIGNMENT

In general, the alignment between hBN and TBLG is not commensurate. The periodic potential term $V(\vec{Q}_i)$ induces a quasiperiodic potential relative to the TBLG superlattice. The spectrum of the TBLG will get broadened, but since the coupling strength between hBN and graphene is much smaller than the band gaps from the flat bands to the other bands in the TBLG system, we can ignore the other bands and only consider an effective description for the flat bands.

The extra hBN layer breaks the $C_2\mathcal{T}$ symmetry of the TBLG system such that there is no obstruction of constructing localized Wannier orbitals using the two bands near charge neutrality in one valley. The low energy effective tight-binding model is obtained in two steps. First, take the m_z term in H_V together with H_{TBLG} and construct localized Wannier orbitals for the two bands in one valley. Second, project the $V(\vec{Q}_i)$ terms to the active bands and transform to Wannier basis.

We use the projection method to obtain Wannier functions [41]. The relationship between Bloch function and Wannier function can be written as

$$\phi^\dagger_{n,\vec{x}_0} = \frac{1}{\sqrt{N}} \sum_{\vec{k},m} e^{-i\vec{k}\cdot\vec{x}_0} \psi^\dagger_{m,\vec{k}} (U_{\vec{k}})_{mn}, \tag{5}$$

where $\phi^\dagger_{n,\vec{x}_0}$ is the creation operator for the Wannier orbital labeled by n at position $\vec{x}_0$, $\psi^\dagger_{m,\vec{k}}$ is the creation operator for the Bloch state, and $m \in \{c, v\}$ labels the conduction band and valence band in one valley. $U_{\vec{k}}$ is a unitary matrix, defined

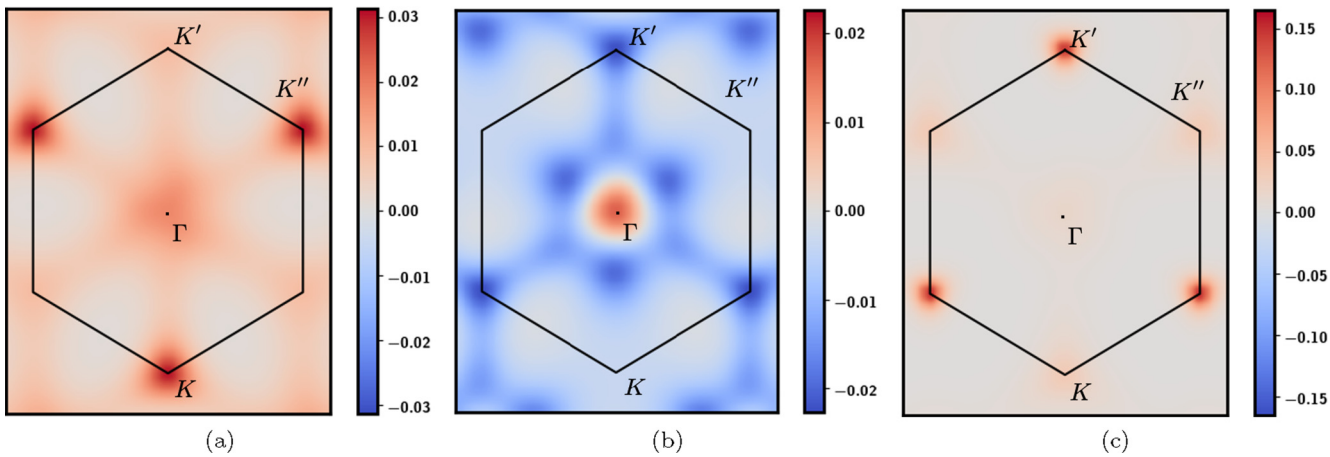

FIG. 4. Berry curvature distribution of valence band for (a) m_z only, (b) Case 1, and (c) Case 2. $\theta_G = 1.2^\circ$. The black line is the boundary of the first BZ and the black dot is the Γ point.

TABLE I. Hopping between the same type of lattice sites.

θ_G	1.2°
t_{0AA}	4.575
t_{0BB}	-1.270
t_{1AA}	$1.547e^{i(-0.197)\pi}$
t_{1BB}	$-1.613e^{i(-0.188)\pi}$
t_{2AA}	$0.482e^{i(-0.349)\pi}$
t_{2BB}	$-0.452e^{i(0.316)\pi}$
t_{3AA}	$0.506e^{i(-0.134)\pi}$
t_{3BB}	$-0.521e^{i(-0.13)\pi}$

TABLE II. Hopping between AB lattice sites.

θ_G	1.2°
t_{1AB}	$2.249e^{i(0.082)\pi}$
t_{2AB}	$-1.54e^{i(0.333)\pi}$
t_{3AB1}	$-0.398e^{i(0.123)\pi}$
t_{3AB2}	$0.668e^{i(-0.304)\pi}$
t_{4AB1}	$-0.412e^{i(0.131)\pi}$
t_{4AB2}	$-0.590e^{i(0.133)\pi}$
t_{5AB}	$-0.270e^{i(0.314)\pi}$
t_{6AB1}	$-0.320e^{i(-0.142)\pi}$
t_{6AB2}	$-0.165e^{i(0.289)\pi}$

as $U_{\vec{k}} = A_{\vec{k}}(A_{\vec{k}}^\dagger A_{\vec{k}})^{-1/2}$, where $(A_{\vec{k}})_{mn} = \langle \mu_m(\vec{k})|g_n(\vec{k})\rangle$ is the overlap matrix between the Bloch wave function $|\mu_m(\vec{k})\rangle$ and k-space representation of a localized wave function ansatz $|g_n(\vec{k})\rangle$. In the numerical calculation below, we take $|g_n(\vec{k})\rangle = e^{-\vec{k}^2/32}e^{-i\vec{k}\cdot\vec{x}_0}|\varphi_n\rangle$ so after inverse Fourier transform, $|g_n(\vec{x})\rangle$ is localized near $\vec{x}_0$. $|\varphi_n\rangle$ is a constant vector in $\vec{k}$ space and it is chosen to maximize the singular values of $A_{\vec{k}}$ [42].

The projected hopping terms and quasiperiodic potential terms can be written as

$$t_{mn}(\vec{x}_{ij}) = \frac{1}{N}\sum_{\vec{k}} e^{i\vec{k}\cdot\vec{x}_{ij}}(U_{\vec{k}}^\dagger \epsilon_{\vec{k}} U_{\vec{k}})_{mn}$$

$$V_{mn}(\vec{x}_i,\vec{x}_j) = \frac{1}{N}\sum_{q=1}^{3} e^{-i\vec{Q}_q\cdot\vec{x}_j}\sum_{\vec{k}} e^{i\vec{k}\cdot\vec{x}_{ij}}(U_{\vec{k}}^\dagger f^q(\vec{k}) U_{\vec{k}+\tilde{\vec{Q}}_q})_{mn}, \quad (6)$$

where $\vec{x}_{ij} = \vec{x}_i - \vec{x}_j$ is the displacement of the two lattice points, $\epsilon_{\vec{k}} = \mathrm{diag}\{\epsilon_c(\vec{k}), \epsilon_v(\vec{k})\}$, $\epsilon_{c,v}(\vec{k})$ being the dispersion of the conduction/valence bands. $\tilde{\vec{Q}}_q$ is defined in the first BZ of the TBLG system and is related to $\vec{Q}_q$ by addition of integer multiples of $\vec{G}_1$ and $\vec{G}_2$. $f^q(\vec{k})$ is the form factor, whose matrix element is

$$f^q_{n_1,n_2}(\vec{k}) = \sum_{mn} \psi^*_{n_1 t,\vec{k}+m\vec{G}_1+n\vec{G}_2}(V_q)_{n_1,n_2}\psi_{n_2 t,\vec{k}+\vec{Q}_q+m\vec{G}_1+n\vec{G}_2}, \quad (7)$$

where $\psi_{n_1 t,\vec{k}}$ denotes the wave function in $\vec{k}$ space of the n_1 sublattice of the top layer graphene and V_q is the coupling matrix of the quasiperiodic potential term, in the form of Eq. (4). The effective Hamiltonian can therefore be written as

$$H_{tb} = \sum_{ij}(t_{mn}(\vec{x}_{ij})c^\dagger_{im}c_{jn} + \mathrm{H.c.}) + \sum_{ij}(V_{mn}(\vec{x}_i,\vec{x}_j)c^\dagger_{im}c_{jn} + \mathrm{H.c.}), \quad (8)$$

where c_i lives on the moiré lattice formed by the TBLG and we can write $\vec{r}_i = n_i\vec{a}_{M1} + m_i\vec{a}_{M2}$, where $\vec{a}_{M1} = a_M(\frac{1}{2}, \frac{\sqrt{3}}{2})$ and $\vec{a}_{M2} = a_M(0,1)$, $a_M = \frac{2a}{\sin(\theta_G/2)}$ being the moiré lattice constant.

After $U_{\vec{k}}$ is obtained, we get t_{mn}'s and V_{mn}'s from Eq. (6). Let us consider t_{mn}'s first. We find that in order to reproduce the band gap and band structure well, we need to keep the hopping terms up to the third nearest unit cell. (See Table I and Table II.) t_{0AA} and t_{0BB} are onsite potentials for sites A and B. The meaning of the other labels is explained in Fig. 5. Without the quasiperiodic terms, the dispersion of H_{tb} is plotted in Fig. 6. The valence and conduction bands have Chern number ± 1, respectively.

Let us consider the V_{mn} terms. There are two effects of the twist angle between hBN and graphene θ_{BN} on the tight-binding Hamiltonian: One is the change of the $\vec{Q}$'s and the other is the change of projected amplitude of the quasiperiodic potential terms. We study two different θ_{BN}'s numerically: $\theta_{\mathrm{BN}} = 0^\circ$ and 0.8°. We project the quasiperiodic terms to the Wannier orbitals and calculate $V_{mn}(\vec{x}_i,\vec{x}_j)$. We find that although the amplitude of the quasiperiodic terms decays with $|\vec{x}_i - \vec{x}_j|$, within the fourth nearest neighbor it is of the order of $\sim$1 meV, which is comparable to the hopping terms. We keep up to the fourth nearest neighbor quasiperiodic terms in the following calculations due to the comparable magnitude of them.

We plot the density of states for $\theta_{\mathrm{BN}} = 0^\circ$ and $\theta_{\mathrm{BN}} = 0.8^\circ$ in Fig. 7. At both angles, there are some small peaks, but those peaks do not form isolated subbands due to the incommensurate nature of the quasiperiodic term. There are eight main peaks for $\theta_{\mathrm{BN}} = 0^\circ$ which can be explained by the

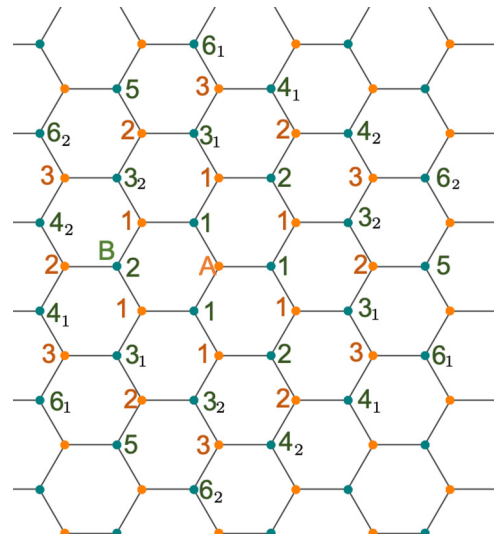

FIG. 5. Labels of the hopping terms from site A (orange circle) to other nearby sites. For example, hopping from A to an orange site labeled '2' corresponds to t_{2AA} and from A to a green site labeled 3_1 corresponds to t_{3AB1}.

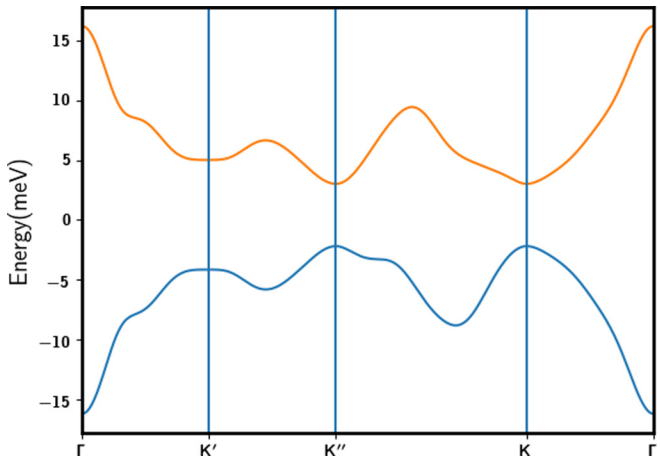

FIG. 6. Dispersion of the effective tight-binding model.

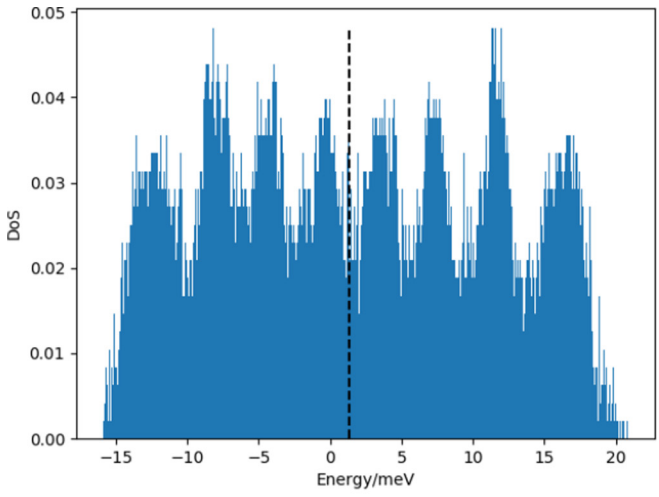

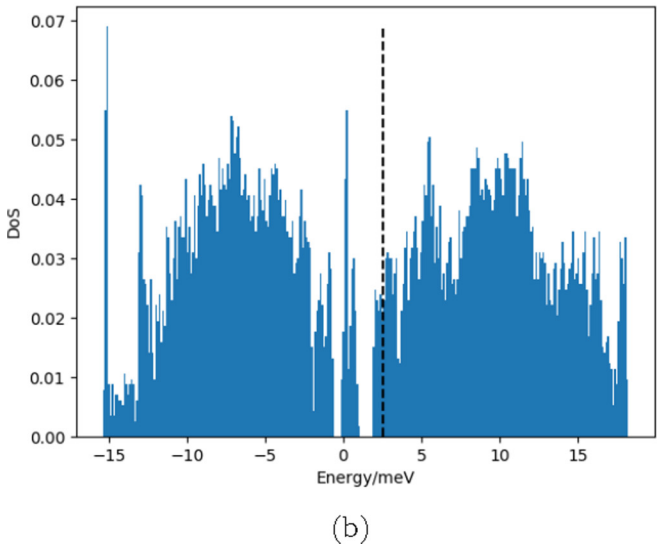

FIG. 7. Density of states at (a) $\theta_{\rm BN} = 0^\circ$ and (b) $\theta_{\rm BN} = 0.8^\circ$ for a 71×71 grid in $\vec{k}$ space. The dotted line indicates the energy of the middle state in the spectrum.

commensurate approximation. We can always find a sequence of rational numbers to approximate an irrational number by means of continued fraction expansion. Let us write $\vec{Q}_{1n} = \frac{s_n}{r_n}\vec{G}_1 + \frac{t_n}{r_n}\vec{G}_2$, where s_n, t_n, r_n are integers and $\lim_{n\to\infty} Q_{1n} = \vec{Q}_1$. For each finite n, the BZ is folded into a mini BZ with reciprocal lattice vectors $(\vec{G}_{1n}, \vec{G}_{2n}) = (\vec{G}_1/r_n, \vec{G}_2/r_n)$ with $2r_n^2$ orbitals at each $\vec{k}$ point. For $\theta_{\rm BN} = 0^\circ$, we get $\vec{Q}_1(\theta_{\rm BN} = 0^\circ) \approx 0.49\vec{G}_1 + 0.47\vec{G}_2$ so the first order approximation is $(s_1, t_1, r_1) = (1, 1, 2)$. Thus, there are roughly eight "bands." The main difference between the two $\theta_{\rm BN}$'s is that for $\theta_{\rm BN} = 0^\circ$, the spectrum is gapless near charge neutrality while it is gapped for $\theta_{\rm BN} = 0.8^\circ$ and the gap size is reduced to $\sim$1 meV compared to $\sim$7 meV without quasiperiodic potential. We then study the localization properties of the states. We introduce PR (participation ratio) in $\vec{k}$ space, PR $= \frac{(\sum_{\vec{k}} |\psi_{\vec{k}}|^2)^2}{\sum_{\vec{k}} |\psi_{\vec{k}}|^4}$ [19]. States that are localized in real space are extended in momentum space and so we expect $|\psi_{\vec{k}}| \sim 1/N$, where $N \times N$ is the system size in $\vec{k}$ space. Thus PR $\sim N^2$ for localized states and PR $\sim$ constant for extended states. From Fig. 8, we find that the PR share similar features as the density of states, which means that near the dips of density of states (DOS), there are more extended states while near the peaks of DOS, there are more localized states. Localized states in $\vec{k}$ space are extended in real space. Thus, we indeed get metallic behavior near charge neutrality for $\theta_{\rm BN} = 0^\circ$ and mobility edges exist.

The density of states indicates that the alignment of hBN has a strong effect on the low energy physics especially near charge neutrality. We then calculate the Hall conductivity σ_{xy} using Kubo formula for one valley and one spin species to further address the difference in electrical transport. In the full many body system, this is the Hall conductivity obtained (within Hartree Fock) if the system is spontaneously fully spin and valley polarized at the filling considered. Thus at 3/4 filling of the conduction band (as appropriate for the experiments of Refs. [7,8], within a Hartree-Fock treatment, full spin-valley polarization leads to full hole filling of one of the Chern bands. This corresponds to placing the effective chemical potential of the Hartree-Fock bands at charge neutrality. We plot σ_{xy} as a function of the effective chemical potential in Fig. 9. For $\theta_{\rm BN} = 0.8^\circ$, σ_{xy} is quantized to $\sim$1 if the chemical potential is slightly below charge neutrality while for $\theta_{\rm BN} = 0^\circ$ it is not quantized.

V. CHERN BANDS WITH QUASIPERIODIC POTENTIAL: A TOY MODEL

The natural occurrence of topological bands and a quasiperiodic potential in TBLG/hBN discussed in previous sections leads to a number of interesting theoretical questions. For ordinary nontopological bands, the question of how different the effects of a quasiperiodic potential are as compared to a random potential on the electronic wave functions has begun to be addressed in recent years [18,43,44]. Here we are interested instead in similar questions when, in addition, the bands are topological. Within a free fermion theory, what is the behavior of the conductivity as a function of chemical potential? As part of addressing this question, it is important to understand in the first place how to couple in an external

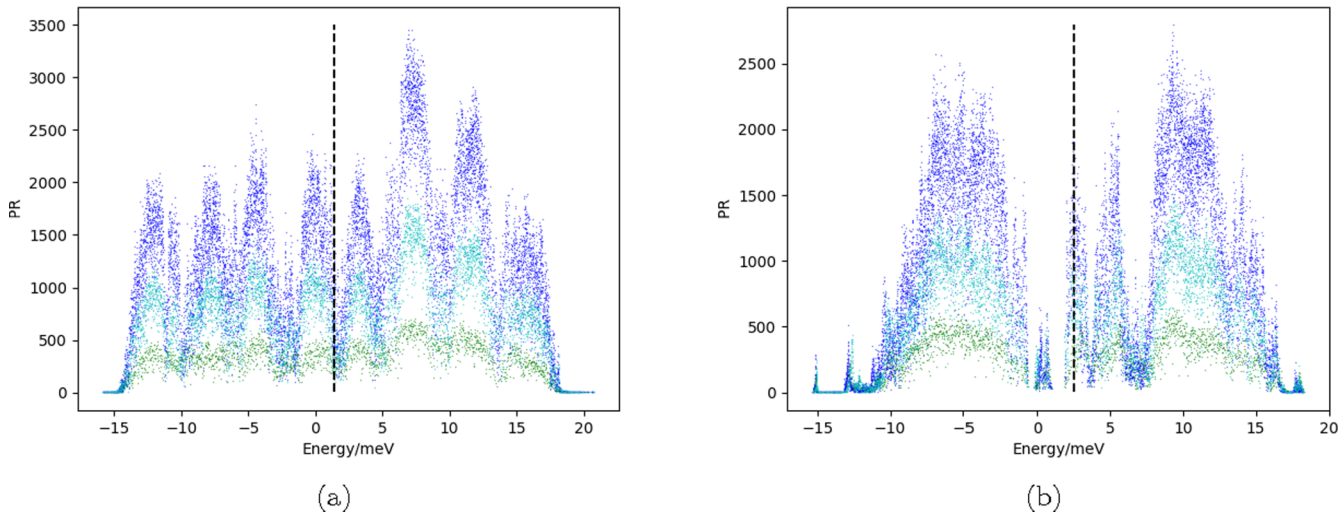

FIG. 8. PR at (a) $\theta_{\rm BN} = 0^\circ$ and (b) $\theta_{\rm BN} = 0.8^\circ$ for different states throughout the entire energy spectrum. The dotted line indicates the energy of the middle state in the spectrum. Different color indicates different system size. From bottom to top: $N = 30, 50, 70$ and the system size is $N \times N$ in $\vec{k}$ space.

vector potential to the electrons in the topological band which is itself a subtle question, as we shall see.

Here we address these questions within a simple context. Let us consider a system with a Chern band and add a quasiperiodic potential to it. If the strength of the quasiperiodic potential is much smaller than the band gaps between the topological band considered and all the other bands, the minimal approach is to project the Hamiltonian to the low energy Chern band. Since there is Wannier obstruction, a tight-binding model in real space is not possible. Thus, we write the effective Hamiltonian in momentum space. For simplicity, assume that we have a flat band to begin with. In momentum space, the Hamiltonian can be written as

$$H = \sum_{\vec{k}} \sum_{\vec{Q}_i} c^\dagger_{\vec{k}} V(\vec{Q}_i) c_{\vec{k}+\vec{Q}_i} \lambda(\vec{k}, \vec{k}+\vec{Q}_i) + \text{H.c.}, \qquad (9)$$

where $\lambda(\vec{k}, \vec{k}+\vec{Q}_i)$ is the form factor and $\vec{Q}_i$'s are the reciprocal vectors for the quasiperiodic potential. For each $\vec{k}$, the Hamiltonian can be viewed as a tight-binding model in momentum space with a lattice generated by $\vec{Q}_i$'s. For $\vec{Q}_i$'s that are incommensurate with the original reciprocal lattice vectors $\vec{G}_{1,2}$ that generate the Brillouin zone, we expect $\vec{k} + n_1\vec{Q}_1 + n_2\vec{Q}_2$ mod $(m_1\vec{G}_1 + m_2\vec{G}_2)$ ($n_{1,2}$ and $m_{1,2}$ are integers) to be dense in the first Brillouin zone. In this case, we only need to consider one lattice that is generated by $\vec{k} + n_1\vec{Q}_1 + n_2\vec{Q}_2$ with a fixed $\vec{k}$. To keep contact with moiré graphene, we will let $\vec{Q}_{1,2}$ generate a triangular lattice, but similar discussion can be carried out on any lattice.

For trivial bands, one can take $\lambda(\vec{k}, \vec{k}+\vec{Q}_i) = 1$. In this case, the eigenvectors are plane waves in $\vec{k}$ space and therefore they are localized in real space. Thus at large quasiperiodic

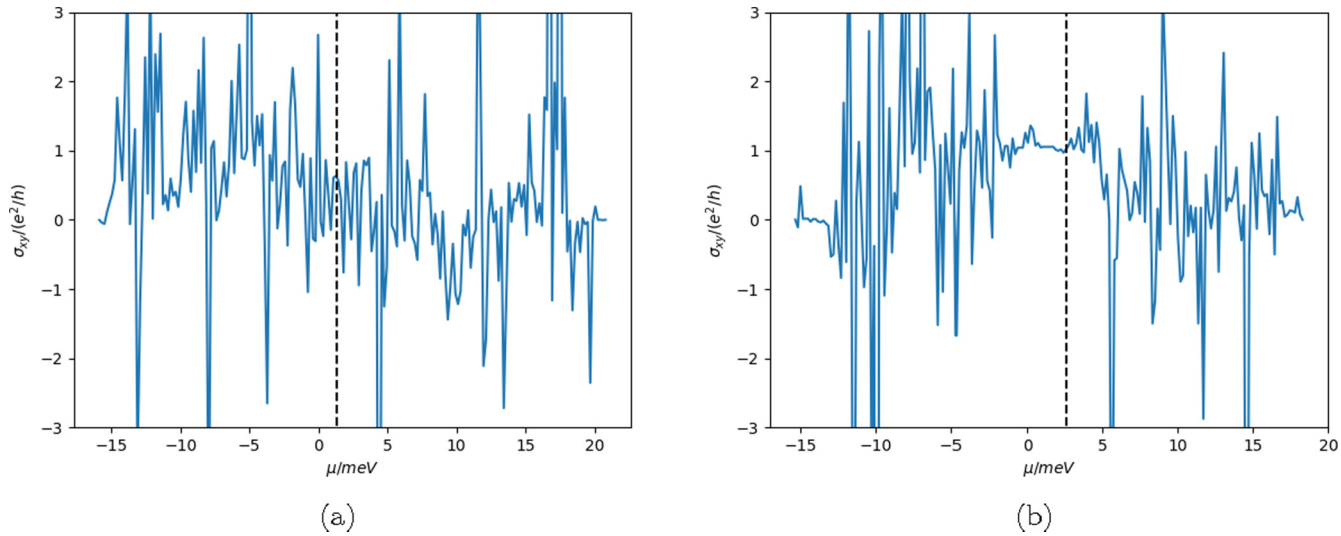

FIG. 9. σ_{xy} vs chemical potential at (a) $\theta_{\rm BN} = 0^\circ$ and (b) $\theta_{\rm BN} = 0.8^\circ$ for a 50×50 grid in $\vec{k}$ space. The dotted line indicates the energy of the middle state in the spectrum.

potential strength for trivial bands, there is always localization.

For a Chern band, on the other hand, the form factor is nontrivial. For small $|\vec{Q}|$, it can be written as $\lambda(\vec{k},\vec{k}+\vec{Q}_i) = F(\vec{k},\vec{k}+\vec{Q}_i)e^{-i\int_{\vec{k}}^{\vec{k}+\vec{Q}_i}\vec{A}(\vec{q})\cdot d\vec{q}}$, where $F(\vec{k},\vec{k}+\vec{Q}_i)$ is real and positive and the path of the integral is taken to be a straight line from $\vec{k}$ to $\vec{k}+\vec{Q}_i$. To simplify the problem, we assume homogeneous Berry curvature and further let $F(\vec{k},\vec{k}+\vec{Q}_i)=1$ for now. Then the Hamiltonian is equivalent to a tight-binding model in a uniform perpendicular magnetic field. We choose Landau gauge such that $\vec{A}(\vec{k}) = (-Bk_y, 0, 0)$. B is proportional to Chern number and the magnetic flux is in general not rational. For this choice of gauge, $\lambda(\vec{k},\vec{k}') = e^{i\frac{B}{2}(k'_x-k_x)(k'_y+k_y)}$. The Hamiltonian can be written as

$$\begin{aligned} H = \sum_{\vec{k}} (&V_1 c^\dagger_{k_x,k_y} c_{k_x+1,k_y} e^{iBk_y} \\ &+ V_2 c^\dagger_{k_x,k_y} c_{k_x-1/2,k_y+\sqrt{3}/2} e^{-i\frac{B}{2}(k_y+\frac{\sqrt{3}}{4})} \\ &+ V_3 c^\dagger_{k_x,k_y} c_{k_x-1/2,k_y-\sqrt{3}/2} e^{-i\frac{B}{2}(k_y-\frac{\sqrt{3}}{4})} + \text{H.c.}), \end{aligned} \quad (10)$$

where the lattice spacing is set to be 1 and $V_{1,2,3}$ are taken to be real. The Hamiltonian in Eq. (10) is a special case of that considered in Ref. [45]. Following the arguments in Ref. [45], we can perform a Fourier transform along the k_x direction. The 2D model is then equivalent to a 1D lattice model with quasiperiodic (QP) potential. One can write $k_y = k_y^0 + n\frac{\sqrt{3}}{2}$, where n is an integer. Note that we assume $\vec{k}$ lattice is dense in the original BZ. We can take k_y^0 to be 0. The flux quanta is $\Phi = \frac{\sqrt{3}B}{4\pi}$. Thus the 1D lattice model with QP potential is

$$E\phi_n = 2V_1\cos(2\pi n\Phi + \nu)\phi_n + A_{n,n+1}\phi_{n+1} + A_{n,n-1}\phi_{n-1}, \quad (11)$$

where $A_{n,n+1} = V_2 e^{-i[\pi\Phi(n+\frac{1}{2})]-i\frac{\nu}{2}} + V_3 e^{i[\pi\Phi(n+\frac{1}{2})]+i\frac{\nu}{2}}$ and $A_{n,n-1} = A^*_{n-1,n}$. $\psi(k_x,k_y)$ is the eigenfunction for the Hamiltonian (10) at energy E, $\psi(k_x,k_y) = e^{ik_x\nu}\phi(k_y)$, and $\phi_n \equiv \phi(k_y^0 + n\frac{\sqrt{3}}{2})$.

Depending on the relative strength of $V_{1,2,3}$, $\phi(k_y)$ can be either localized or extended in k_y space. If there is C_3 rotational symmetry, which corresponds to $V_1 = V_2 = V_3$, the 1D system is at the critical point of the localization transition and thus the eigenstates are not localized in real space, which is different from the trivial band case.

If the C_3 symmetry is broken, we get the Lyapunov exponent (inverse of the localization length) by considering three different gauge choices, i.e., along the three axes of the triangular lattice [45,46] and the Lyapunov exponent $\lambda(E;V_1,V_2,V_3)$ for ϕ_n in Eq. (11) is

$$\lambda(E;V_1,V_2,V_3) = ln\left(\frac{|V_1|}{|V_3|}\right), \quad (12)$$

if $|V_1| \geqslant |V_3| \geqslant |V_2|$, and

$$\lambda(E;V_1,V_2,V_3) = ln\left(\frac{|V_1|}{|V_2|}\right), \quad (13)$$

if $|V_1| \geqslant |V_2| \geqslant |V_3|$. $\lambda(E;V_1,V_2,V_3) = 0$ otherwise.

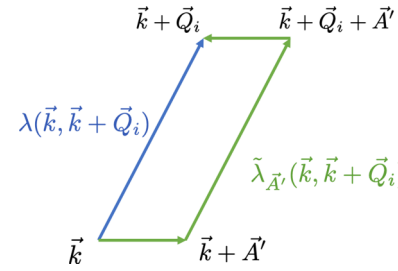

FIG. 10. Schematic of the line integrals in Eq. (14).

Even though we get localized or extended $\psi(k_x,k_y)$, depending on the choices of $V_{1,2,3}$, we still need to address the question of what effect it will have on the physical observables. Thus, we study the DC transport of the system in the following.

In the trivial case, all the states are localized so we expect the conductance to vanish. In the topological case, we need to couple the tight-binding Hamiltonian in k space to external electric field. First we need to obtain current operators in the presence of external electric field. The strategy is to apply a probe vector potential $\vec{A}'$ and $J_\mu = -\frac{\partial H[\vec{E},\vec{A}']}{\partial A'_\mu}|_{A'_\mu\to 0}$. The vector potential $\vec{A}'$ will "shift" the momenta $\vec{k}$. We have to be careful about what we mean by "shift." In comparison to the trivial band, there is a gauge structure in k space. If we change $c_{\vec{k}}$ to $c_{\vec{k}}e^{i\theta(\vec{k})}$ and $\vec{A}(\vec{k})$ to $\vec{A}(\vec{k}) + \partial_{\vec{k}}\theta(\vec{k})$, where $\theta(\vec{k})$ is a differentiable function in $\vec{k}$, $c^\dagger_{\vec{k}}c_{\vec{k}+\vec{Q}}\lambda(\vec{k},\vec{k}+\vec{Q})$ is invariant. In order to keep the gauge invariance of the theory, we cannot simply replace $\lambda(\vec{k},\vec{k}')$ by $\lambda(\vec{k}+\vec{A}',\vec{k}'+\vec{A}')$. The only gauge-invariant deformation of the form factor $\lambda(\vec{k},\vec{k}')$ is to attach a small plaquette with Berry curvature as flux. This generalizes the idea of Peierls substitution. Again, let us only consider the phase factor in the form factor for now. The gauge invariant change in the form factor $\lambda(\vec{k},\vec{k}+\vec{Q}_i)$ by shifting the momentum by $\vec{A}'$ is

$$\tilde{\lambda}_{\vec{A}'}(\vec{k},\vec{k}+\vec{Q}_i) - \lambda(\vec{k},\vec{k}+\vec{Q}_i) = \lambda(\vec{k},\vec{k}+\vec{Q}_i)e^{iB(\vec{Q}_i\times\vec{A}')\cdot\hat{e}_z}, \quad (14)$$

where $\tilde{\lambda}_{\vec{A}'}(\vec{k},\vec{k}+\vec{Q}_i)$ denotes the shifted form factor and it is defined as the Wilson loop of the Berry connection along the green curve in Fig. 10. $\hat{e}_z$ is the directional vector along the z axis.

The way that we construct the coupling to the external vector potential in Eq. (14) seems to rely on the specific form of the form factor $\lambda(\vec{k},\vec{k}+\vec{Q})$. For a generic form factor, we also construct the gauge coupling (see Appendix B for details), which agrees with Eq. (14).

The tight-binding Hamiltonian coupled to the probe vector potential and external electric field can be written as

$$\begin{aligned} H[\vec{E},\vec{A}'] = \sum_{\vec{k}} \big(&V_1 c^\dagger_{k_x,k_y} c_{k_x+1,k_y} e^{iBk_y} e^{iBA'_y} \\ &+ V_2 c^\dagger_{k_x,k_y} c_{k_x-1/2,k_y+\sqrt{3}/2} e^{-i\frac{B}{2}(k_y+\frac{\sqrt{3}}{4}+A'_y)} e^{-iB\frac{\sqrt{3}}{2}A'_x} \\ &+ V_3 c^\dagger_{k_x,k_y} c_{k_x-1/2,k_y-\sqrt{3}/2} e^{-i\frac{B}{2}(k_y-\frac{\sqrt{3}}{4}+A'_y)} e^{iB\frac{\sqrt{3}}{2}A'_x} + \text{H.c.}\big) \\ &+ V(\vec{E},\vec{A}'). \end{aligned} \quad (15)$$

$V(\vec{E},\vec{A}') = \int d^2x\vec{E}\cdot\vec{x}\rho(\vec{x};\vec{A}')$ is the electric potential, where $\rho(\vec{x};\vec{A}')$ is the density operator. In k space, we define the Fourier transformation of $\rho(\vec{x};\vec{A}')$ as $\rho(\vec{q};\vec{A}')$ and

$$\begin{aligned}\rho(\vec{q};\vec{A}') &= \sum_{\vec{k}} c^\dagger_{\vec{k}} c_{\vec{k}+\vec{q}}\lambda(\vec{k},\vec{k}+\vec{q})e^{iB(\vec{q}\times\vec{A}')\cdot\hat{e}_z} \\ &= \rho(\vec{q};\vec{A}'=0)e^{iB(\vec{q}\times\vec{A}')\cdot\hat{e}_z}. \end{aligned} \tag{16}$$

Thus the electric potential can be written as

$$\begin{aligned} V(\vec{E},\vec{A}') &= \iint d^2qd^2x\vec{E}\cdot\vec{x}\rho(\vec{q};\vec{A}'=0)e^{-i\vec{q}\cdot(\vec{x}-B\vec{A}'\times\hat{e}_z)} \\ &= V(\vec{E},\vec{A}'=0) + B\vec{E}\cdot(\vec{A}'\times\hat{e}_z)\rho(\vec{q}=0;\vec{A}'=0) \end{aligned} \tag{17}$$

to linear order in B, and the probe vector field $\vec{A}'$ only couples to the second term above.

We can do a sanity check of the above expression. Suppose there's no quasiperiodic potential; we can get $J_{x,0} = -1/S\sum_{\vec{k}} c^\dagger_{\vec{k}} c_{\vec{k}} BE_y$ and $J_{y,0} = 1/S\sum_{\vec{k}} c^\dagger_{\vec{k}} c_{\vec{k}} BE_x$, where S is the total area of the system. For a fully-filled Chern band with Chern number C, $B = \frac{2\pi C}{A_{\rm BZ}} = \frac{CA_{\rm cell}}{2\pi}$, where $A_{\rm BZ}(A_{\rm cell})$ is the area of the Brillouin zone (unit cell). Thus the Hall conductivity $\sigma_{xy} = \frac{B}{A_{\rm cell}} = \frac{C}{2\pi}$ is quantized.

Now that we have some confidence in the Peierls substitution, let us take the quasiperiodic potential into account. The current density operators can be expressed as

$$\begin{aligned} J_x = \frac{1}{S}\sum_{\vec{k}}\Bigg(& i\frac{\sqrt{3}}{2}V_2 B c^\dagger_{k_x,k_y} c_{k_x-1/2,k_y+\sqrt{3}/2} e^{-i\frac{B}{2}(k_y+\frac{\sqrt{3}}{4})} \\ & - i\frac{\sqrt{3}}{2}V_3 B c^\dagger_{k_x,k_y} c_{k_x-1/2,k_y-\sqrt{3}/2} e^{-i\frac{B}{2}(k_y-\frac{\sqrt{3}}{4})} + \text{H.c.}\Bigg) \\ & - \frac{1}{S}\sum_{\vec{k}} c^\dagger_{\vec{k}} c_{\vec{k}} BE_y \\ J_y = -\frac{1}{S}\sum_{\vec{k}}\Bigg(& iBV_1 c^\dagger_{k_x,k_y} c_{k_x+1,k_y} e^{iBk_y} \\ & - i\frac{B}{2}V_2 c^\dagger_{k_x,k_y} c_{k_x-1/2,k_y+\sqrt{3}/2} e^{-i\frac{B}{2}(k_y+\frac{\sqrt{3}}{4})} \\ & - i\frac{B}{2}V_3 c^\dagger_{k_x,k_y} c_{k_x-1/2,k_y-\sqrt{3}/2} e^{-i\frac{B}{2}(k_y-\frac{\sqrt{3}}{4})} + \text{H.c.}\Bigg) \\ & + \frac{1}{S}\sum_{\vec{k}} c^\dagger_{\vec{k}} c_{\vec{k}} BE_x. \end{aligned} \tag{18}$$

Let us consider $E_x = E$ and $E_y = 0$. The transport properties are the same as a tight-binding model in real space if we view k_x as the y coordinate, and k_y as the x coordinate. By making this mapping, we transform the problem of nontrivial Berry curvature in $\vec{k}$ space to the problem of a real-space tight-binding model under perpendicular magnetic field. In the original model, $\vec{E}$ is along the x direction while $\vec{E}$ is along the y direction in the real-space model. This is the same as what happens in lowest Landau level (LLL). Indeed, if we view the wave functions for the LLL as wave functions for the flat Chern band at $C = 1$ and calculate the form factors, by comparing with Ref. [47], we get the drift current exactly in the form of Eq. (18).

For commensurate flux $\Phi = 2p/q$, translational symmetry is restored and the energy spectrum is divided into q magnetic subbands. For simplicity, we only consider zero temperature. $\sigma_{xx} = 0$ if the chemical potential is within band gaps. σ_{xy} can be obtained through the TKNN formula [48],

$$\sigma_{xy} = \sum_m \int \frac{d^2\nu}{(2\pi)^2} f_m(\vec{\nu})\left[\mathcal{F}_m(\vec{\nu}) + \frac{C}{2\pi}\right], \tag{19}$$

where $m \in \{1,\ldots,q\}$ is the index of magnetic bands, and $f_m(\vec{\nu})$ is the Fermi-Dirac distribution. $\vec{\nu}$ takes value with the magnetic Brillouin zone $\nu_x \in (-\pi,\pi]$ and $\nu_y \in (-\pi/q,\pi/q]$. $\mathcal{F}_m(\vec{\nu}) + \frac{C}{2\pi}$ is the total Berry curvature of the states at $\vec{\nu}$ of the mth band, where the first term takes care of the contribution of the QP potential and the second term comes from the background Berry curvature.

Note that σ_{xy} is quantized although it is not obvious from the expression in Eq. (19). Following Refs. [48,49], Eq. (19) is reduced to $\sigma_{xy} = \frac{mC}{2\pi}$, where m is an integer that satisfies the diophantine equation $-p\Delta n + qm = 1$, where Δn is an integer.

For incommensurate flux, by mapping to the real-space model, $\sigma_{xx} = 0$ if the filled states are localized along the k_y direction, which is the case for $|V_1| > \max(|V_2|,|V_3|)$. Otherwise, if $|V_1| < \max(|V_2|,|V_3|)$, all states are extended.

Let us consider σ_{xy} next. If the chemical potential is within the gap and the gap is not closed, if we continuously tune the value of Φ from an irrational number to a nearby rational number $\Phi_0 = 2p/q$, the value of σ_{xy} is then completely determined by the Berry curvature of the filled bands at Φ_0. The exact value of Φ_0 is determined by the details of the energetics.

So far, we have only considered flat bands. We can further include the kinetic terms $\epsilon_{\vec{k}} c^\dagger_{\vec{k}} c_{\vec{k}}$. $\epsilon_{\vec{k}}$ is the dispersion, which is a periodic function in $\vec{k}$ and $\epsilon_{\vec{k}} = \epsilon_{\vec{k}+m\vec{G}_1+n\vec{G}_2}$, where $\vec{G}_{1,2}$ are the reciprocal lattice vectors and m,n are integers. Note that $\vec{G}_{1,2}$ are in general not commensurate with the reciprocal vectors of the quasiperiodic potential $\vec{Q}_{1,2}$ so the kinetic terms act as onsite "quasiperiodic" terms of the tight-binding Hamiltonian in $\vec{k}$ space. Roughly speaking, whether an eigenstate is localized or extended is given by the competition between hopping terms and onsite quasiperiodic (QP) potential terms, i.e., the competition between the energy scales of the bandwidth and of the onsite QP potential. We have shown that Berry curvature plays a role of magnetic field in $\vec{k}$ space and for a tight-binding model under magnetic field, the energy spectrum can in general develop several subbands even if Φ is irrational, as in Hofstadter's butterfly [50]. The relevant energy scale for the kinetic energy in $\vec{k}$ space is thus the bandwidth of the magnetic subbands, which is reduced from the bandwidth of the same tight-binding model but with no Berry curvature. In this sense, it is "easier" to get localized states in $\vec{k}$ space, that is, extended states in real space in a topological band rather than in a trivial band under onsite QP potential.

With dispersion and (or) nonuniformity of the Berry curvature taken into account, the Hamiltonian written in $\vec{k}$ space cannot be reduced to an equivalent 1D Hamiltonian and one cannot use the Thouless formula to obtain the localization

length. Nonetheless, we expect that there is at least one state in the spectrum that is extended or critical in real space due to the nontrivial topology of the original Chern band. We also calculate the inverse participate ratio (IPR $= \frac{\sum_{\vec{k}} |\psi_{\vec{k}}|^4}{(\sum_{\vec{k}} |\psi_{\vec{k}}|^2)^2}$) numerically for different system sizes and find that there are more *nonlocalized* states (extended or critical) for the nontrivial Berry curvature case than for the vanishing Berry curvature case (see Appendix D for details).

We can take one step further towards the TBLG aligned with the hBN system by considering two flat topological bands with Chern number ± 1. For illustration purpose, we only consider a square lattice; the quasiperiodic potential only contains the lowest harmonics and the system has C_4 rotational symmetry. The quasiperiodic potential also only acts within the same band and there is an interband mixing term. The Hamiltonian thus can be written as

$$\begin{aligned} H_{\pm} = & \frac{\Delta}{2} \sum_{\vec{k}} (c^{\dagger}_{\vec{k};+} c_{\vec{k};+} - c^{\dagger}_{\vec{k};-} c_{\vec{k};-}) \\ & + V_0 \sum_{\vec{k},\vec{Q}} c^{\dagger}_{\vec{k};\pm} c_{\vec{k}+\vec{Q};\pm} \lambda_{\pm\pm}(\vec{k}, \vec{k}+\vec{Q}) \\ & + V_1 \sum_{\vec{k}} c^{\dagger}_{\vec{k};+} c_{\vec{k};-} \lambda^0_{+-}(\vec{k}) + \text{H.c.}, \end{aligned} \tag{20}$$

where the subscripts $\pm$ label the different bands. The V_0 terms are projected quasiperiodic potential terms, and the V_1 terms are interband hopping between the two $\pm$ Chern bands. The form factor $\lambda_{\pm\pm}(\vec{k}, \vec{k}+\vec{Q}) = \langle \psi_{\vec{k};\pm} | e^{-i\vec{Q}\cdot\vec{x}} | \psi_{\vec{k}+\vec{Q};\pm} \rangle$, where $|\psi_{\vec{k};\pm}\rangle$ are Bloch states and similarly, $\lambda^0_{+-}(\vec{k}) = \langle \psi_{\vec{k};+} | \psi_{\vec{k};-} \rangle$. Δ is set to be positive. For the purpose of illustration, we take $|\psi_{\vec{k};a}\rangle$ to be the same as in the LLL and choose a Landau gauge $\vec{A}_{\pm} = (\mp By, 0)$ such that $\langle \vec{x} | \psi_{\vec{k};\pm} \rangle = \sum_m e^{i(\mp m k_y + k_x x + mBx \mp k_x k_y/B)} \Psi_0(y \pm \frac{k_x + mB}{B})$ (see Appendix C for details), where $\Psi_0(y) = (\frac{B}{\pi})^{\frac{1}{4}} e^{-\frac{By^2}{2}}$. We further let $\vec{Q}_1 = Q(2\pi, 0)$ and $\vec{Q}_2 = Q(0, 2\pi)$, where Q is an irrational number [note that in LLL, we can always define the magnetic Brillouin zone so $\vec{Q}_{1,2}$ are aligned with the mBZ reciprocal lattice vectors $\vec{G}_{1,2}$, which are set to be $(2\pi, 0)$ and $(0, 2\pi)$ here]. As elaborated in Appendix C, the form factors are

$$\begin{aligned} \lambda_{\pm\pm}(\vec{k}, \vec{k}+\vec{Q}) &= e^{\mp i \frac{2k_y Q_x + Q_x Q_y}{2B} - \frac{4\pi^2 Q^2}{4B}} \\ \lambda^0_{+-}(\vec{k}) &= \sum_{m=-\infty}^{\infty} e^{\frac{2ik_y}{B}(k_x + mB) - \frac{(k_x+mB)^2}{B}}. \end{aligned} \tag{21}$$

Plugging in the definition of $\vec{Q}_1$ and $\vec{Q}_2$, we have, $\lambda_{\pm\pm}(\vec{k}, \vec{k}+\vec{Q}_1) = e^{-\frac{\pi Q^2}{2} \mp i Q k_y}$ and $\lambda_{\pm\pm}(\vec{k}, \vec{k}+\vec{Q}_2) = e^{-\frac{\pi Q^2}{2}}$.

One can check that the $c_{\vec{k};\pm}$ bands are topological bands with Chern number ± 1 in two ways. First, by taking derivatives of $\vec{Q}$ in Eq. (21) around $\vec{Q} = 0$, one gets uniform Berry curvature of $\pm\frac{1}{B}$ for $c_{\vec{k};\pm}$ bands, respectively. Second, since the phases of the Bloch wave functions $|\psi_{\vec{k};\pm}\rangle$ are well defined in the whole BZ, the integration of Berry curvature over the BZ is reduced to a contour integral of the Berry connection along the boundary of the BZ. We have $|\psi_{(k_x+2\pi,k_y);\pm}\rangle = |\psi_{(k_x,k_y);\pm}\rangle$ and $|\psi_{(k_x,k_y+2\pi);\pm}\rangle = e^{\pm i k_x} |\psi_{(k_x,k_y);\pm}\rangle$ such that $\vec{\mathcal{A}}_{(\pi,k_y);\pm} = \vec{\mathcal{A}}_{(-\pi,k_y);\pm}$ and $\vec{\mathcal{A}}_{(k_x,\pi);\pm} = \vec{\mathcal{A}}_{(k_x,-\pi);\pm} \mp \hat{\mathbf{e}}_x$, where $\vec{\mathcal{A}}_{(k_x,k_y);\pm}$ is the Berry connection and $\hat{\mathbf{e}}_x$ is the unit vector along k_x. Thus the contour integrals of $\vec{\mathcal{A}}_{\vec{k};\pm}$ along the boundary of the BZ yield Chern number ± 1.

If $V_0 = 0$, the Hamiltonian in Eq. (20) is block diagonal in $\vec{k}$ space. By solving the 2×2 block, we have the two eigenvalues $\pm\epsilon_{\vec{k}} = \pm\sqrt{\frac{\Delta^2}{4} + V_1^2 |\lambda^0_{+-}(\vec{k})|^2}$ so the system is always gapped if $\Delta \neq 0$ and has a gap that is $\geqslant \Delta$. The eigenvectors are

$$\begin{aligned} d_{\vec{p};+} &= \sqrt{\frac{\epsilon_{\vec{p}} + \Delta/2}{2\epsilon_{\vec{p}}}} c_{\vec{p};+} + e^{i\theta(\vec{p})} \sqrt{\frac{\epsilon_{\vec{p}} - \Delta/2}{2\epsilon_{\vec{p}}}} c_{\vec{p};-} \\ d_{\vec{p};-} &= -e^{-i\theta(\vec{p})} \sqrt{\frac{\epsilon_{\vec{p}} - \Delta/2}{2\epsilon_{\vec{p}}}} c_{\vec{p};+} + \sqrt{\frac{\epsilon_{\vec{p}} + \Delta/2}{2\epsilon_{\vec{p}}}} c_{\vec{p};-}, \end{aligned} \tag{22}$$

where $d_{\pm}$ are the annihilation operators for eigenstates in $\pm$ energy bands and $\theta(\vec{p}) = Arg[\lambda^0_{+-}(\vec{p})]$. We choose the phase factors such that in the limit of $V_1 \to 0$, $d_{\vec{p};\pm} \to c_{\vec{p};\pm}$. Since the V_1 term does not close the gap, we expect the $d_{\vec{k};\pm}$ bands to have the same Chern number as the $c_{\vec{k};\pm}$ bands. Note that $\lambda^0_{+-}(\vec{k}) = 0$ at $(k_x, k_y) = (\pm\pi, \pm\frac{\pi}{2})$ and $\theta(\vec{k})$ is not well defined at these singular points. However, the factors associated with $\theta(\vec{k})$ in Eq. (22) vanish at $(k_x, k_y) = (\pm\pi, \pm\frac{\pi}{2})$ so the $d_{\vec{k};\pm}$ fields can be continuously defined in the whole BZ.

If $V_1 = 0$, $c_{\vec{k},+}$ and $c_{\vec{k},-}$ bands are decoupled and each one of the bands is a flat band with QP. As we discussed before, the spectrum of each band has fractal structure and the width of the spectrum is of the order of V_0. Moreover, from Eq. (20), after a partial Fourier transformation along k_x, we find that the V_0 terms are the same for $c_{\vec{k};+}$'s and $c_{\vec{k};-}$'s. Thus the energy spectra of $\pm$ bands are identical and the "+" bands are shifted with an energy Δ from the "−" bands, with the same corresponding energy eigenstates. If $V_0 \ll \Delta$, there is a band gap between the two "fractal" bands that consist of $c_{\vec{k},\pm}$ degrees of freedom, respectively, and we get a Chern insulator at half filling. If $V_0 \sim \Delta$, the gap at half filling will close. If $V_0 \gg \Delta$, the fractal bands contributing positive Hall conductivity and negative Hall conductivity almost overlap, resulting in nearly zero Hall conductivity.

Now we take both V_0 and V_1 into account. If we fix V_1 and Δ and increase V_0, the band gap decreases and eventually vanishes. We further calculate the IPR (see Appendix D for details). We find that there are extended states (in real space) near band edges when the band gap is not closed. Upon increasing V_0, after the band gap closes, there are localized states near zero energy. Similar "leviation" and "pair annihilation" behavior of the extended states is also observed in disordered topological insulators [51,52]. If the strength of QP potential further increases, the states near zero energy get delocalized since in the $V_0 \gg V_1$ limit, the model reduces to two decoupled AA models at critical points.

VI. CONCLUSION

In this paper we showed that when magic-angle twisted bilayer graphene is nearly aligned with hBN, the single particle physics is sensitive to the quasiperiodic potential produced by the interference between two moiré potentials: one produced by the relative twist of the two graphene layers and the other

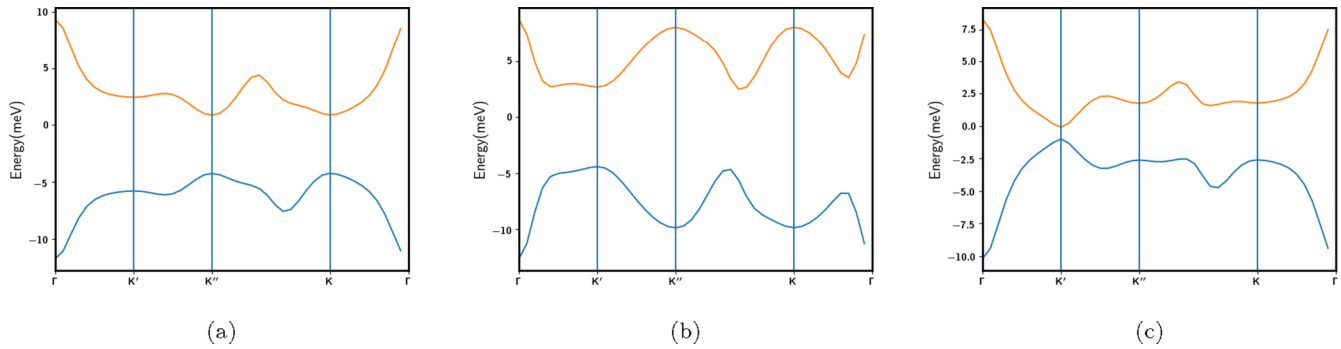

FIG. 11. Dispersion for (a) only m_z, (b) Case 1, and (c) Case 2. $\theta_G = 1.15°$.

produced by the hBN substrate. The periodic modulation induced by hBN cannot be treated as a small perturbation due to the narrow bandwidth of the valence and conduction bands. By exact diagonalization, we find that for TBLG twist angle 1.2°, for alignment angle $\theta_{\mathrm{BN}} = 0°$ and $\theta_{\mathrm{BN}} = 0.8°$, localized states and extend states are both present and there is no clear mobility edge. For $\theta_{\mathrm{BN}} = 0°$, the charge gap near neutrality is closed. In the presence of valley polarization (due to interactions), the Hall conductivity σ_{xy} is not quantized when $\theta_{\mathrm{BN}} = 0°$ while for $\theta_{\mathrm{BN}} = 0.8°$, the charge gap is reduced and σ_{xy} is quantized.

In order to study the electron properties of topological bands in the presence of quasiperiodic potential, it is more straightforward to begin with a model in momentum space since the nontriviality is manifest in the form factor. In the limit of flat band and uniform Berry curvature, we find that quasiperiodic potential induces hopping between different momentum, which can be mapped to a tight-binding model coupled to magnetic field. We discussed localization properties and transport in such toy models. The next step will be to introduce dispersion and electron-electron interaction, which we leave for future studies.

ACKNOWLEDGMENTS

We thank Anushya Chandran, Zhihuan Dong, David Goldhaber-Gordon, Pablo Jarillo-Herrero, and Ya-Hui Zhang for useful discussions. This work was supported by NSF Grant No. DMR-1911666, and partially through a Simons Investigator Award from the Simons Foundation to Senthil Todadri. This work was also partly supported by the Simons Collaboration on Ultra-Quantum Matter, which is a grant from the Simons Foundation (651440, TS).

APPENDIX A: NUMERICAL RESULTS FOR $\theta_G = 1.15°$

1. Perfect alignment

We plot the dispersion in Fig. 11 and berry curvature distribution of the valence band in Fig. 12.

2. Incommensurate alignment

We study the density of states and PR for $\theta_G = 1.15°$ and $\theta_{\mathrm{BN}} = -0.6°$, which is close to perfect alignment. Indeed we find a clear gap near charge neutrality and there is no indication of localization from PR (see Fig. 13).

APPENDIX B: MINIMAL COUPLING IN A TOPOLOGICAL BAND

The gauge transformation operator can be written as

$$U = e^{i\int_{\vec{q}}\theta(\vec{q},\tau)\rho(\vec{q})}, \tag{B1}$$

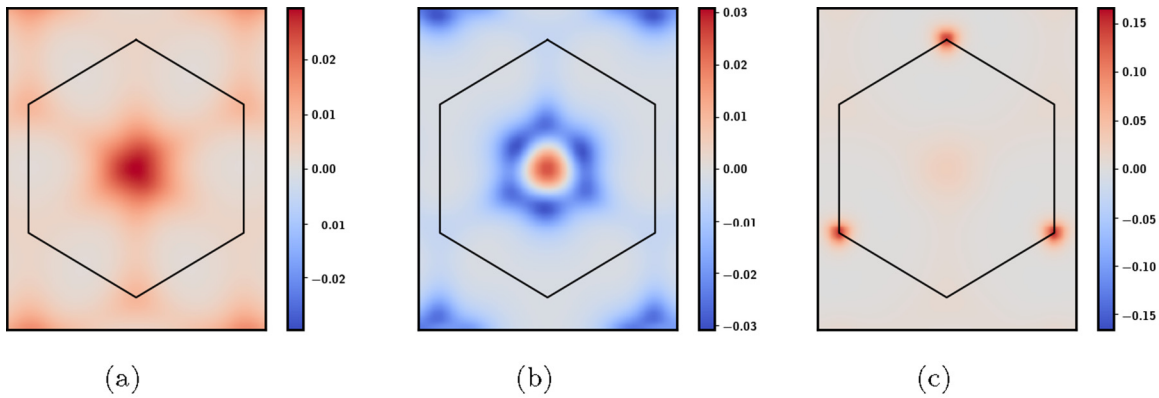

FIG. 12. Berry curvature distribution of the valence band for (a) only m_z, (b) Case 1, and (c) Case 2. $\theta_G = 1.15°$.

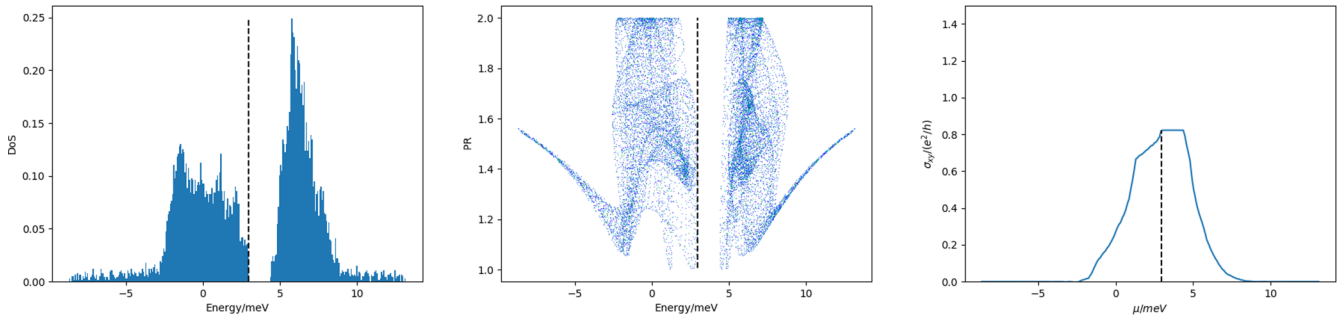

(a) (b) (c)

FIG. 13. Density of states, PR, and σ_{xy} for $\theta_G = 1.15^\circ$ and $\theta_{\mathrm{BN}} = -0.6^\circ$.

where $\rho(\vec{q})$ is the projected density operator in momentum space,

$$\rho(\vec{q}) = \int \frac{d^2k}{(2\pi)^2} c^\dagger_{\vec{k}-\vec{q}} c_{\vec{k}} \lambda(\vec{k}, \vec{q}). \tag{B2}$$

$\lambda(\vec{k}, \vec{q}) = \langle u_{\vec{k}} | u_{\vec{k}-\vec{q}} \rangle$ is the form factor (note that the definition is different from the main text), and $\theta(\vec{q}, \tau)$ is the Fourier transform of a real function $\theta(\vec{x}, \tau)$, so $\theta(\vec{q}, \tau)^* = \theta(-\vec{q}, \tau)$.

For an infinitesimal gauge transformation, $U \approx 1 + i \int_{\vec{q}} \theta(\vec{q}, \tau) \rho(\vec{q})$ and an operator $\hat{O} \to U^\dagger \hat{O} U$ under gauge transformation. Thus we have

$$U^\dagger c_{\vec{k}} U \approx c_{\vec{k}} + i \int_{\vec{q}} \theta(\vec{q}, \tau) \lambda(\vec{k} + \vec{q}, \vec{q}) c_{\vec{k}+\vec{q}}$$
$$U^\dagger c^\dagger_{\vec{k}} U \approx c^\dagger_{\vec{k}} - i \int_{\vec{q}} \theta(\vec{q}, \tau) \lambda(\vec{k}, \vec{q}) c^\dagger_{\vec{k}-\vec{q}}. \tag{B3}$$

Consider an action in Euclidean signature that contains three terms, $\mathcal{S}_0 = \int d^2k \int d\tau c^\dagger_{\vec{k}} \partial_\tau c_{\vec{k}} - \epsilon_{\vec{k}} c^\dagger_{\vec{k}} c_{\vec{k}} - \sum_{\vec{Q}} V_{\vec{Q}} \rho_{\vec{Q}}$, where $\vec{Q}$ does not need to be commensurate with the reciprocal lattice vector. Performing a gauge transformation to these terms, we have

$$\begin{aligned}
\delta\left(\int_{\vec{k}} c^\dagger_{\vec{k}} \partial_\tau c_{\vec{k}}\right) &\approx -i \int_{\vec{k},\vec{q}} \theta(\vec{q}, \tau) \lambda(\vec{k}, \vec{q}) c^\dagger_{\vec{k}-\vec{q}} \partial_\tau c_{\vec{k}} + i \int_{\vec{k},\vec{q}} c^\dagger_{\vec{k}} \partial_\tau [\theta(\vec{q}, \tau) \lambda(\vec{k} + \vec{q}, \vec{q}) c_{\vec{k}+\vec{q}}] \\
&= i \int_{\vec{k},\vec{q}} [\partial_\tau \theta(\vec{q}, \tau)] \lambda(\vec{k}, \vec{q}) c^\dagger_{\vec{k}-\vec{q}} c_{\vec{k}} \\
\delta\left(\int_{\vec{k}} \epsilon_{\vec{k}} c^\dagger_{\vec{k}} c_{\vec{k}}\right) &\approx -i \int_{\vec{k},\vec{q}} \theta(\vec{q}, \tau) \lambda(\vec{k}, \vec{q}) c^\dagger_{\vec{k}-\vec{q}} \epsilon_{\vec{k}} c_{\vec{k}} + i \int_{\vec{k},\vec{q}} c^\dagger_{\vec{k}} \epsilon_{\vec{k}} \theta(\vec{q}, \tau) \lambda(\vec{k} + \vec{q}, \vec{q}) c_{\vec{k}+\vec{q}} \\
&= i \int_{\vec{k},\vec{q}} \theta(\vec{q}, \tau) \lambda(\vec{k}, \vec{q}) c^\dagger_{\vec{k}-\vec{q}} c_{\vec{k}} (\epsilon_{\vec{k}-\vec{q}} - \epsilon_{\vec{k}}) \\
\delta(V_{\vec{Q}} \rho_{\vec{Q}}) &\approx -i V_{\vec{Q}} \int_{\vec{k},\vec{q}} \lambda(\vec{k}, \vec{Q}) \theta(\vec{q}, \tau) \lambda(\vec{k} - \vec{Q}, \vec{q}) c^\dagger_{\vec{k}-\vec{q}-\vec{Q}} c_{\vec{k}} + i V_{\vec{Q}} \int_{\vec{k},\vec{q}} \lambda(\vec{k}, \vec{Q}) c^\dagger_{\vec{k}-\vec{Q}} \theta(\vec{q}, \tau) \lambda(\vec{k} + \vec{q}, \vec{q}) c_{\vec{k}+\vec{q}} \\
&= i V_{\vec{Q}} \int_{\vec{k},\vec{q}} \theta(\vec{q}, \tau) c^\dagger_{\vec{k}-\vec{q}-\vec{Q}} c_{\vec{k}} [\lambda(\vec{k} - \vec{q}, \vec{Q}) \lambda(\vec{k}, \vec{q}) - \lambda(\vec{k}, \vec{Q}) \lambda(\vec{k} - \vec{Q}, \vec{q})].
\end{aligned} \tag{B4}$$

If we further consider long wavelength gauge transformation, we only need to take small $\vec{q}$ in $\theta(\vec{q}, \tau)$ into account. Note that $\partial_{\vec{k}} \epsilon_{\vec{k}} = \vec{v}_{\vec{k}}$ and

$$\lambda(\vec{k} - \vec{q}, \vec{Q}) \lambda(\vec{k}, \vec{q}) - \lambda(\vec{k}, \vec{Q}) \lambda(\vec{k} - \vec{Q}, \vec{q}) = -\vec{q} \cdot [\vec{\partial}_{\vec{k}} \lambda(\vec{k}, \vec{Q}) + i \lambda(\vec{k}, \vec{Q}) (\vec{\mathcal{A}}_{\vec{k}} - \vec{\mathcal{A}}_{\vec{k}-\vec{Q}})] + o(q^2), \tag{B5}$$

where $\vec{\mathcal{A}}_{\vec{k}} = -i \langle u_{\vec{k}} | \partial_{\vec{k}} u_{\vec{k}} \rangle$ is the Berry connection in momentum space. Thus, the change in action $\mathcal{S}_0$ can be written as

$$\begin{aligned}
\delta \mathcal{S}_0 = \int d\tau \int_{\vec{k},\vec{q}} (i \partial_\tau \theta(\vec{q}, \tau) + i \vec{q} \cdot \vec{v}_{\vec{k}} \theta(\vec{q}, \tau)) \lambda(\vec{k}, \vec{q}) c^\dagger_{\vec{k}-\vec{q}} c_{\vec{k}} + \sum_{\vec{Q}} i V_{\vec{Q}} \int_{\vec{k},\vec{q}} \theta(\vec{q}, \tau) c^\dagger_{\vec{k}-\vec{q}-\vec{Q}} c_{\vec{k}} \vec{q} \\
\cdot [\vec{\partial}_{\vec{k}} \lambda(\vec{k}, \vec{Q} + \vec{q}) + i \lambda(\vec{k}, \vec{Q} + \vec{q}) (\vec{\mathcal{A}}_{\vec{k}} - \vec{\mathcal{A}}_{\vec{k}-\vec{Q}-\vec{q}})] + o(q^2).
\end{aligned} \tag{B6}$$

Now let us consider the electromagnetic potential $A(\vec{q},\tau)=(A_0,\vec{A})$. Note that the projection to the topological band should only affect the gauge transformation of the projected degrees of freedom and the gauge transformation of the electromagnetic potential should remain the same as before the projection. Thus under a gauge transformation, we have

$$A_0(\vec{q},\tau)\to A_0(\vec{q},\tau)-\partial_\tau\theta(\vec{q},\tau)$$
$$\vec{A}(\vec{q},\tau)\to\vec{A}(\vec{q},\tau)+i\vec{q}\,\theta(\vec{q},\tau). \tag{B7}$$

The goal is to construct terms involving the electromagnetic potential $A(\vec{q},\tau)$ such that $\delta\mathcal{S}_0$ can be canceled by the gauge transformation of the $A(\vec{q},\tau)$ field. As a first attempt, we consider the following action

$$\begin{aligned}\mathcal{S}_1=&\int d\tau\int_{\vec{k},\vec{q}}(iA_0(\vec{q},\tau)-\vec{A}(\vec{q},\tau)\cdot\vec{v}_{\vec{k}})\lambda(\vec{k},\vec{q})c^\dagger_{\vec{k}-\vec{q}}c_{\vec{k}}\\&-\int d\tau\int_{\vec{k},\vec{q}}\vec{A}(\vec{q},\tau)\cdot\sum_{\vec{Q}}V_{\vec{Q}}c^\dagger_{\vec{k}-\vec{q}-\vec{Q}}c_{\vec{k}}[\vec{\partial}_{\vec{k}}\lambda(\vec{k},\vec{Q}+\vec{q})\\&+i\lambda(\vec{k},\vec{Q}+\vec{q})(\vec{\mathcal{A}}_{\vec{k}}-\vec{\mathcal{A}}_{\vec{k}-\vec{Q}-\vec{q}})].\end{aligned} \tag{B8}$$

Note that $\delta\mathcal{S}_0$ is canceled by terms in $\delta\mathcal{S}_1$ but there are other terms in $\delta\mathcal{S}_1$, so we have

$$\delta\mathcal{S}_1=-\delta\mathcal{S}_0+\delta\mathcal{S}_1' \tag{B9}$$

and

$$\begin{aligned}-i\delta\mathcal{S}_1'=&\int d\tau\int_{\vec{k},\vec{q},\vec{q}'}(iA_0(\vec{q},\tau)-\vec{A}(\vec{q},\tau)\cdot\vec{v}_{\vec{k}})\lambda(\vec{k},\vec{q})[-c^\dagger_{\vec{k}-\vec{q}-\vec{q}'}c_{\vec{k}}\theta(\vec{q}',\tau)\lambda(\vec{k}-\vec{q},\vec{q}')+c^\dagger_{\vec{k}-\vec{q}}c_{\vec{k}+\vec{q}'}\theta(\vec{q}',\tau)\lambda(\vec{k}+\vec{q}',\vec{q}')]\\&-\int d\tau\int_{\vec{k},\vec{q},\vec{q}'}\vec{A}(\vec{q},\tau)\cdot\sum_{\vec{Q}}V_{\vec{Q}}[\vec{\partial}_{\vec{k}}\lambda(\vec{k},\vec{Q}+\vec{q})+i\lambda(\vec{k},\vec{Q}+\vec{q})(\vec{\mathcal{A}}_{\vec{k}}-\vec{\mathcal{A}}_{\vec{k}-\vec{Q}-\vec{q}})]\\&\times[-c^\dagger_{\vec{k}-\vec{q}-\vec{Q}-\vec{q}'}c_{\vec{k}}\theta(\vec{q}',\tau)\lambda(\vec{k}-\vec{q}-\vec{Q},\vec{q}')+c^\dagger_{\vec{k}-\vec{q}-\vec{Q}}c_{\vec{k}+\vec{q}'}\theta(\vec{q}',\tau)\lambda(\vec{k}+\vec{q}',\vec{q}')]\\=&\int d\tau\int_{\vec{k},\vec{q},\vec{q}'}iA_0(\vec{q},\tau)c^\dagger_{\vec{k}-\vec{q}-\vec{q}'}c_{\vec{k}}\theta(\vec{q}',\tau)[\lambda(\vec{k},\vec{q}')\lambda(\vec{k}-\vec{q}',\vec{q})-\lambda(\vec{k}-\vec{q},\vec{q}')\lambda(\vec{k},\vec{q})]\\&-\int d\tau\int_{\vec{k},\vec{q},\vec{q}'}A_\mu(\vec{q},\tau)c^\dagger_{\vec{k}-\vec{q}-\vec{q}'}c_{\vec{k}}\theta(\vec{q}',\tau)[v^\mu_{\vec{k}-\vec{q}'}\lambda(\vec{k},\vec{q}')\lambda(\vec{k}-\vec{q}',\vec{q})-v^\mu_{\vec{k}}\lambda(\vec{k}-\vec{q},\vec{q}')\lambda(\vec{k},\vec{q})]\\&-\int d\tau\int_{\vec{k},\vec{q},\vec{q}'}\vec{A}(\vec{q},\tau)\cdot\sum_{\vec{Q}}V_{\vec{Q}}c^\dagger_{\vec{k}-\vec{q}-\vec{Q}-\vec{q}'}c_{\vec{k}}\theta(\vec{q}',\tau)\{[\vec{\partial}_{\vec{k}-\vec{q}'}\lambda(\vec{k}-\vec{q}',\vec{Q}+\vec{q})+i\lambda(\vec{k}-\vec{q}',\vec{Q}+\vec{q})(\vec{\mathcal{A}}_{\vec{k}-\vec{q}'}-\vec{\mathcal{A}}_{\vec{k}-\vec{q}'-\vec{Q}-\vec{q}})]\\&\times\lambda(\vec{k},\vec{q}')-[\vec{\partial}_{\vec{k}}\lambda(\vec{k},\vec{Q}+\vec{q})+i\lambda(\vec{k},\vec{Q}+\vec{q})(\vec{\mathcal{A}}_{\vec{k}}-\vec{\mathcal{A}}_{\vec{k}-\vec{Q}-\vec{q}})]\lambda(\vec{k}-\vec{q}-\vec{Q},\vec{q}')\}\\\approx&-\int d\tau\int_{\vec{k},\vec{q},\vec{q}'}(iA_0(\vec{q},\tau)-\vec{A}(\vec{q},\tau)\cdot\vec{v}_{\vec{k}})c^\dagger_{\vec{k}-\vec{q}-\vec{q}'}c_{\vec{k}}\theta(\vec{q}',\tau)\vec{q}'\cdot[\vec{\partial}_{\vec{k}}\lambda(\vec{k},\vec{q})+i\lambda(\vec{k},\vec{q})(\vec{\mathcal{A}}_{\vec{k}}-\vec{\mathcal{A}}_{\vec{k}-\vec{q}})]\\&+\int d\tau\int_{\vec{k},\vec{q},\vec{q}'}A_\mu(\vec{q},\tau)c^\dagger_{\vec{k}-\vec{q}-\vec{q}'}c_{\vec{k}}\theta(\vec{q}',\tau)\lambda(\vec{k},\vec{q}+\vec{q}')\vec{q}'\cdot\vec{\partial}_{\vec{k}}v^\mu_{\vec{k}}\\&-\int d\tau\int_{\vec{k},\vec{q},\vec{q}'}\vec{A}(\vec{q},\tau)\cdot\sum_{\vec{Q}}V_{\vec{Q}}c^\dagger_{\vec{k}-\vec{q}-\vec{Q}-\vec{q}'}c_{\vec{k}}\theta(\vec{q}',\tau)\{-(\vec{q}'\cdot\vec{\partial}_{\vec{k}})\vec{\partial}_{\vec{k}}\lambda(\vec{k},\vec{Q}+\vec{q})-i\vec{q}'\cdot\vec{\partial}_{\vec{k}}[\lambda(\vec{k},\vec{Q}+\vec{q})(\vec{\mathcal{A}}_{\vec{k}}-\vec{\mathcal{A}}_{\vec{k}-\vec{Q}-\vec{q}})]\\&+[\vec{\partial}_{\vec{k}}\lambda(\vec{k},\vec{Q}+\vec{q})+i\lambda(\vec{k},\vec{Q}+\vec{q})(\vec{\mathcal{A}}_{\vec{k}}-\vec{\mathcal{A}}_{\vec{k}-\vec{Q}-\vec{q}})]i\vec{q}'\cdot(\vec{\mathcal{A}}_{\vec{k}-\vec{q}-\vec{Q}}-\vec{\mathcal{A}}_{\vec{k}})\}+o((q')^2)\\\approx&\,i\int d\tau\int_{\vec{k},\vec{q},\vec{q}'}(iA_0(\vec{q},\tau)-\vec{A}(\vec{q},\tau)\cdot\vec{v}_{\vec{k}})c^\dagger_{\vec{k}-\vec{q}-\vec{q}'}c_{\vec{k}}\lambda(\vec{k},\vec{q}+\vec{q}')\theta(\vec{q}',\tau)\vec{q}'\times\vec{q}\cdot\hat{z}\mathcal{B}_{\vec{k}}\\&+\int d\tau\int_{\vec{k},\vec{q},\vec{q}'}A_\mu(\vec{q},\tau)c^\dagger_{\vec{k}-\vec{q}-\vec{q}'}c_{\vec{k}}\theta(\vec{q}',\tau)\lambda(\vec{k},\vec{q}+\vec{q}')\vec{q}'\cdot\vec{\partial}_{\vec{k}}v^\mu_{\vec{k}}\\&-\int d\tau\int_{\vec{k},\vec{q},\vec{q}'}\sum_{\vec{Q}}V_{\vec{Q}}c^\dagger_{\vec{k}-\vec{Q}-\vec{q}-\vec{q}'}c_{\vec{k}}\theta(\vec{q}',\tau)[\vec{q}'\cdot(-i\vec{\partial}_{\vec{k}}+\vec{\mathcal{A}}_{\vec{k}}-\vec{\mathcal{A}}_{\vec{k}-\vec{Q}-\vec{q}-\vec{q}'})]\\&\times[\vec{A}(\vec{q},\tau)\cdot(-i\vec{\partial}_{\vec{k}}+\vec{\mathcal{A}}_{\vec{k}}-\vec{\mathcal{A}}_{\vec{k}-\vec{Q}-\vec{q}-\vec{q}'})]\lambda(\vec{k},\vec{Q}+\vec{q}+\vec{q}')+o((q')^2)+o(q^2),\end{aligned} \tag{B10}$$

where $\mathcal{B}_{\vec{k}}=\partial_{k_x}\mathcal{A}_{\vec{k},y}-\partial_{k_y}\mathcal{A}_{\vec{k},x}$ is the Berry curvature.

Now, let us further consider the possible terms that cancel $\delta\mathcal{S}_1'$. Suppose there is $\mathcal{S}_2$, and

$$\begin{aligned}-i\mathcal{S}_2 = &-\int d\tau \int_{\vec{k},\vec{q},\vec{q}'} iA_0(\vec{q},\tau)(\vec{A}(\vec{q}',\tau)\times\vec{q})\cdot\hat{z}c^\dagger_{\vec{k}-\vec{q}-\vec{q}'}c_{\vec{k}}\lambda(\vec{k},\vec{q}+\vec{q}')\mathcal{B}_{\vec{k}}\\ &+\int d\tau\int_{\vec{k},\vec{q},\vec{q}'}(1/2(\partial_\tau\vec{A}(\vec{q},\tau)\times\vec{A}(\vec{q}',\tau)))\cdot\hat{z}c^\dagger_{\vec{k}-\vec{q}-\vec{q}'}c_{\vec{k}}\lambda(\vec{k},\vec{q}+\vec{q}')\mathcal{B}_{\vec{k}}\\ &+\int d\tau\int_{\vec{k},\vec{q},\vec{q}'}A_\mu(\vec{q},\tau)c^\dagger_{\vec{k}-\vec{q}-\vec{q}'}c_{\vec{k}}\lambda(\vec{k},\vec{q}+\vec{q}')iA_\nu(\vec{q}',\tau)\partial_{k_\nu}v^\mu_{\vec{k}}/2+(\vec{A}(\vec{q},\tau)\cdot\vec{v}_{\vec{k}})(\vec{A}(\vec{q}',\tau)\times\vec{q})\cdot\hat{z}c^\dagger_{\vec{k}-\vec{q}-\vec{q}'}c_{\vec{k}}\lambda(\vec{k},\vec{q}+\vec{q}')\mathcal{B}_{\vec{k}}\\ &+\frac{-i}{2}\int d\tau\int_{\vec{k},\vec{q},\vec{q}'}\sum_{\vec{Q}}V_{\vec{Q}}c^\dagger_{\vec{k}-\vec{Q}-\vec{q}-\vec{q}'}c_{\vec{k}}\{\vec{A}(\vec{q}',\tau)\cdot[-i\vec{\partial}_{\vec{k}}+\vec{\mathcal{A}}_{\vec{k}}-\vec{\mathcal{A}}_{\vec{k}-\vec{Q}-\vec{q}-\vec{q}'}]\}\\ &\times\{\vec{A}(\vec{q},\tau)\cdot[-i\vec{\partial}_{\vec{k}}+\vec{\mathcal{A}}_{\vec{k}}-\vec{\mathcal{A}}_{\vec{k}-\vec{Q}-\vec{q}-\vec{q}'}]\}\lambda(\vec{k},\vec{Q}+\vec{q}+\vec{q}').\end{aligned}\tag{B11}$$

One can verify that $\delta\mathcal{S}_2$ cancels $\delta\mathcal{S}_1'$ for small $\vec{q}$ and $\vec{q}'$.

The first two terms in Eq. (B11) can be combined to a Chern-Simons(CS) term. To see this, define $\phi_{\mathcal{B}}(\vec{q}) = \int_{\vec{k}} c^\dagger_{\vec{k}-\vec{q}}c_{\vec{k}}\lambda(\vec{k},\vec{q})\mathcal{B}_{\vec{k}}$ and in real space, the first two terms in Eq. (B11) reduce to

$$\frac{1}{2}\int d\tau\int d^2x\phi_{\mathcal{B}}(-\vec{x})A(\vec{x},\tau)dA(\vec{x},\tau),\tag{B12}$$

where $\phi_{\mathcal{B}}(\vec{x})$ is the Fourier transformation of $\phi_{\mathcal{B}}(\vec{q})$.

As a sanity check, consider a Chern insulator. The ground state expectation value of $\phi_{\mathcal{B}}(\vec{x})$ is $\langle\phi_{\mathcal{B}}(\vec{x})\rangle_{G.S.} = \frac{C}{2\pi}$, where C is the Chern number. This gives the correct quantized coefficient for the CS term.

Thus, at long wavelength, the action for a topological band that is minimally coupled to gauge field is

$$\mathcal{S}[A] = \mathcal{S}_0 + \mathcal{S}_1[A] + \mathcal{S}_2[A].\tag{B13}$$

The current density operator is $\vec{J} = \frac{\delta\mathcal{L}}{\delta\vec{A}}$. Let us consider applying an external static electric field and choose a gauge such that $\vec{E} = -\vec{\nabla}A_0(\vec{x},t)$ and $\vec{A}(\vec{x},t) = 0$. The current density operator around $\vec{q} = 0$ is thus

$$\begin{aligned}J^\mu(-\vec{q}) \approx &-\int_{\vec{k}} v^\mu_{\vec{k}}c^\dagger_{\vec{k}-\vec{q}}c_{\vec{k}}\lambda(\vec{k},\vec{q}) - \phi_{\mathcal{B}}(\vec{q}=0)\epsilon_{\mu\nu}E^\nu\\ &-i\sum_{\vec{Q}}V_{\vec{Q}}\int_{\vec{k}}c^\dagger_{\vec{k}-\vec{Q}-\vec{q}}c_{\vec{k}}\left[-i\partial^\mu_{\vec{k}}+\left(\mathcal{A}^\mu_{\vec{k}}-\mathcal{A}^\mu_{\vec{k}-\vec{Q}-\vec{q}}\right)\right]\\ &\times\lambda(\vec{k},\vec{Q}+\vec{q}).\end{aligned}\tag{B14}$$

For a flat topological band, $\vec{v}_{\vec{k}} = 0$ so the total current $\vec{\mathcal{J}}$ is

$$\begin{aligned}\mathcal{J}^\mu &= J^\mu(\vec{q}=0)\\ &= -\epsilon^{\mu\nu}\sum_{\vec{k}}c^\dagger_{\vec{k}}c_{\vec{k}}\mathcal{B}_{\vec{k}}E_\nu - i\sum_{\vec{Q}}V_{\vec{Q}}\sum_{\vec{k}}c^\dagger_{\vec{k}-\vec{Q}}c_{\vec{k}}\left[-i\partial^\mu_{\vec{k}}\right.\\ &\quad\left.+\left(\mathcal{A}^\mu_{\vec{k}}-\mathcal{A}^\mu_{\vec{k}-\vec{Q}}\right)\right]\lambda(\vec{k},\vec{Q}).\end{aligned}\tag{B15}$$

In the main text, we take $\lambda(\vec{k},\vec{Q}) = e^{i\int_{\vec{k}}^{\vec{k}-\vec{Q}}\vec{\mathcal{A}}}$ so we have

$$\begin{aligned}&\left[-i\partial^\mu_{\vec{k}}+\left(\mathcal{A}^\mu_{\vec{k}}-\mathcal{A}^\mu_{\vec{k}-\vec{Q}}\right)\right]\lambda(\vec{k},\vec{Q})\\ &\quad=\lambda(\vec{k},\vec{Q})\int_{\vec{k}}^{\vec{k}-\vec{Q}}\mathcal{B}(\vec{k}')\epsilon^{\mu\nu}dk'_\nu.\end{aligned}\tag{B16}$$

If the Berry curvature is uniform, the above expression will reduce to $-\epsilon^{\mu\nu}Q_\nu\lambda(\vec{k},\vec{Q})\mathcal{B}$ so we find that Eq. (B15) agrees with Eq. (18) in the main text. To conclude, in the derivation of Eq. (B15) we do not assume any specific form of $\lambda(\vec{k},\vec{Q})$ so the expression of the current operator can be used in any topological band with nontrivial Berry curvature.

APPENDIX C: BLOCH WAVE FUNCTION IN LLL AND FORM FACTORS

In a Landau gauge $\vec{A} = (-By, 0)$, the magnetic translation operators are

$$\begin{aligned}T_x &= e^{iP_x}\\ T_y &= e^{i(P_y+Bx)}.\end{aligned}\tag{C1}$$

One can verify that $[T_x, T_y] = 0$ and T_x, T_y commute with the kinetic momenta $\vec{P}-\vec{A}$, since the magnetic flux $\Phi = B = 2\pi$, where we set the lattice constant to 1.

The eigenfunction $\psi(\vec{x})$ of $T_{x,y}$ can be labeled by the momenta (k_x, k_y) such that the eigenvalues are $e^{ik_{x,y}}$. In order to construct such eigenfunctions, we first examine how $T_{x,y}$ act on a wave function in LLL, that is $\phi_{k_x}(\vec{x}) = e^{ik_xx}\Psi_0(y+\frac{k_x}{B})$, where $\Psi_0(y) = (\frac{B}{\pi})^{\frac{1}{4}}e^{-\frac{By^2}{2}}$. It is readily seen that $\phi_{k_x}(\vec{x})$ is an eigenfunction of T_x and $T_y\phi_{k_x}(\vec{x}) = \phi_{k_x+B}(\vec{x})$. Thus the eigenfunction of $T_{x,y}$ can be written as

$$\begin{aligned}\psi_{\vec{k}}(\vec{x}) &= \sum_{m=-\infty}^{\infty}e^{-imk_y-ik_xk_y/B}\phi_{k_x+mB}(\vec{x})\\ &= \sum_{m=-\infty}^{\infty}e^{i(k_xx+mBx-mk_y-k_xk_y/B)}\Psi_0\left(y+\frac{k_x}{B}+m\right),\end{aligned}\tag{C2}$$

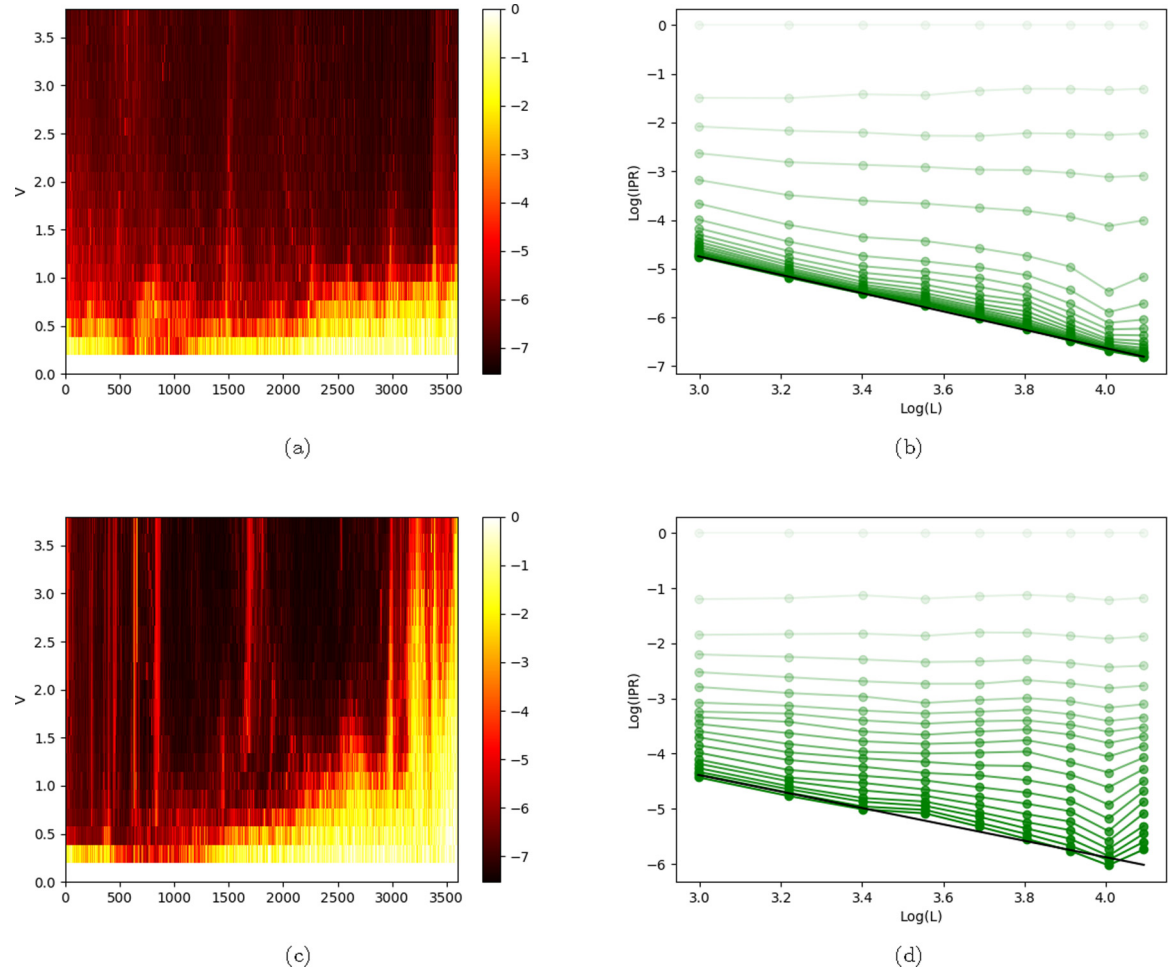

FIG. 14. IPR for single band model with dispersion. (a), (b) trivial case. (c), (d) nontrivial case. In (a), (b), Log(IPR) is plotted; the x axis labels different eigenstates in ascending order of their energies and the y axis labels different QP potential V from 0 to 4. The system size is 60×60. In (b), (d), green dots with different brightness connected by the same line label different QP potential V, from 0 to 4 (top to bottom), with 0.2 interval. The black line is the linear fitting for $V = 4$. The linear system sizes are from 20 to 60.

where m is an integer. Note that we choose a gauge in $\vec{k}$ space such that $\psi_{(k_x,k_y+2\pi)}(\vec{x}) = e^{-ik_x}\psi_{(k_x,k_y)}(\vec{x})$ and $\psi_{(k_x+2\pi,k_y)}(\vec{x}) = \psi_{(k_x,k_y)}(\vec{x})$.

For an opposite magnetic field, we can choose a Landau gauge such that $\tilde{\vec{A}} = (By, 0)$. Then the wave function in the LLL can be written as $\tilde{\phi}_{k_x}(\vec{x}) = e^{ik_x x}\Psi_0(y - \frac{k_x}{B})$. The magnetic translation operators are $\tilde{T}_x = T_x$, $\tilde{T}_y = e^{i(P_y - Bx)}$ so the corresponding eigenfunction can be written as

$$\tilde{\psi}_{\tilde{k}}(\vec{x}) = \sum_{m=-\infty}^{\infty} e^{imk_y + ik_x k_y/B}\tilde{\phi}_{k_x+mB}(\vec{x}) = \sum_{m=-\infty}^{\infty} e^{i(k_x x + mBx + mk_y + k_x k_y/B)}\Psi_0\left(y - \frac{k_x}{B} - m\right). \quad \text{(C3)}$$

Now let us consider various form factors,

$$\begin{aligned}
\lambda_{\pm\pm}(\vec{k}, \vec{k}+\vec{Q}) &= \sum_{m,m'}\int dx \int dy e^{\mp i(k_x Q_y + Q_x k_y + Q_x Q_y)/B - i(mB - m'B)x \mp im'(k_y + Q_y) \pm imk_y - iQ_y y} \\
&\quad \times \Psi_0\left(y \pm \frac{k_x + mB}{B}\right)\Psi_0\left(y \pm \frac{k_x + m'B + Q_x}{B}\right) \\
&= \sum_{m}\int dy e^{\mp i(k_x Q_y + Q_x k_y + Q_x Q_y)/B \mp imQ_y - iQ_y y}\Psi_0\left(y \pm \frac{k_x + mB}{B}\right)\Psi_0\left(y \pm \frac{k_x + mB + Q_x}{B}\right) \\
&= \sum_{m}\int dy e^{\mp i(k_x Q_y + Q_x k_y + Q_x Q_y)/B \mp imQ_y}\left[\Psi_0\left(y \pm \frac{(k_x + mB)}{B} + \frac{\pm Q_x + iQ_y}{2B}\right)\right]^2 e^{-B(\frac{Q_x}{2B})^2 + B(\frac{\pm Q_x + iQ_y}{2B})^2} e^{\pm\frac{(k_x+mB)iQ_y}{B}} \\
&= e^{\mp i\frac{k_y Q_x}{B} \mp \frac{iQ_x Q_y}{2B} - \frac{Q_x^2 + Q_y^2}{4B}}. \quad \text{(C4)}
\end{aligned}$$

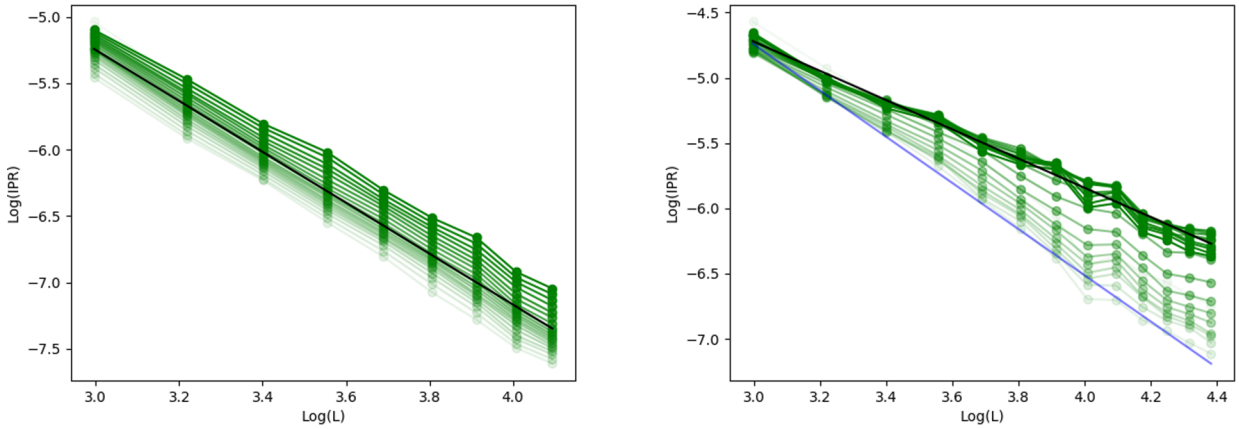

FIG. 15. IPR for single band model with nonuniform Berry curvature. (a) trivial ($B_0 = 0$) and (b) nontrivial ($B_0 \approx 7.26$). Green dots with different brightness connected by the same line label different B_1, from 0 to 4 (top to bottom), with 0.2 interval. The black line in (a) is the linear fitting of the average IPR. The black line in (b) is the linear fitting of the average IPR for $B_1 \geqslant 2$ and the blue line in (b) is the linear fitting for $B_1 = 0.2$.

Now let us consider $\lambda^0_{+-}(\vec{k}) = \langle \psi_{\vec{k};+} | \psi_{\vec{k};-} \rangle$.

$$\lambda^0_{+-}(\vec{k}) = \sum_m \int dy e^{im2k_y + i2k_x k_y/B} \Psi_0\left(y + \frac{k_x + mB}{B}\right) \times \Psi_0\left(y - \frac{k_x + mB}{B}\right)$$
$$= \sum_m \int dy e^{im2k_y + i2k_x k_y/B} [\Psi_0(y)]^2 e^{-B(\frac{k_x+mB}{B})^2}$$
$$= \sum_m e^{2i\frac{k_y}{B}(k_x+mB) - \frac{(k_x+mB)^2}{B}}. \quad \text{(C5)}$$

APPENDIX D: INVERSE PARTICIPATION RATIO OF VARIOUS SYSTEMS

1. IPR of single band models

We consider the Hamiltonian in Eq. (10) with $V_1 = V_2 = V_3 = V$ and further include a dispersion term $H_{dis} = \sum_{\vec{k}} c^\dagger_{\vec{k}} c_{\vec{k}} \epsilon_{\vec{k}}$, where we take $\epsilon_{\vec{k}} = t \sum_{j=1}^3 \cos(\vec{k} \cdot \vec{b}_j)$. $\vec{b}_j$'s are the lattice vectors, taken to be $\vec{b}_1 = \frac{4\pi Q}{\sqrt{3}}(0, -1)$ and $\vec{b}_{2,3} = \frac{4\pi Q}{\sqrt{3}}(\pm\frac{\sqrt{3}}{2}, \frac{1}{2})$. We take the QP lattice to be parallel to the original lattice and Q is an irrational number. We calculate the IPR for various QP potential strength V and system sizes (Fig. 14) given $t = 1$ and $Q = \sqrt{5} - 1$. We compare the system with vanishing Berry curvature (trivial) and uniform Berry curvature given by a $C = 1$ band (nontrivial).

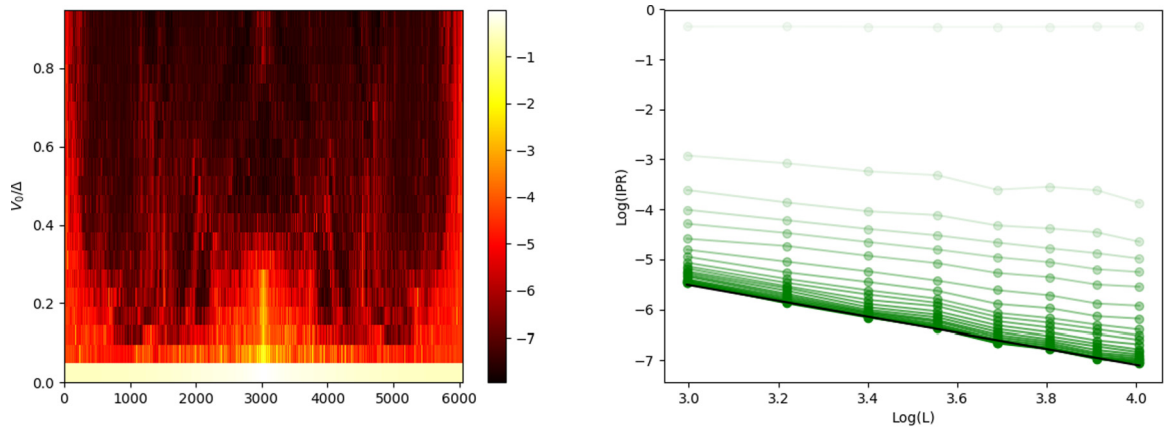

FIG. 16. IPR for the two band model. (a) Color plot of Log(IPR). The x axis labels different eigenvalues. (b) Dependence of Log(IPR) with linear system size. The green lines from bright to dark label different V_0 from 0 to 1. The black line is the linear fitting to the Log(IPR) at $V_0 = 1$.

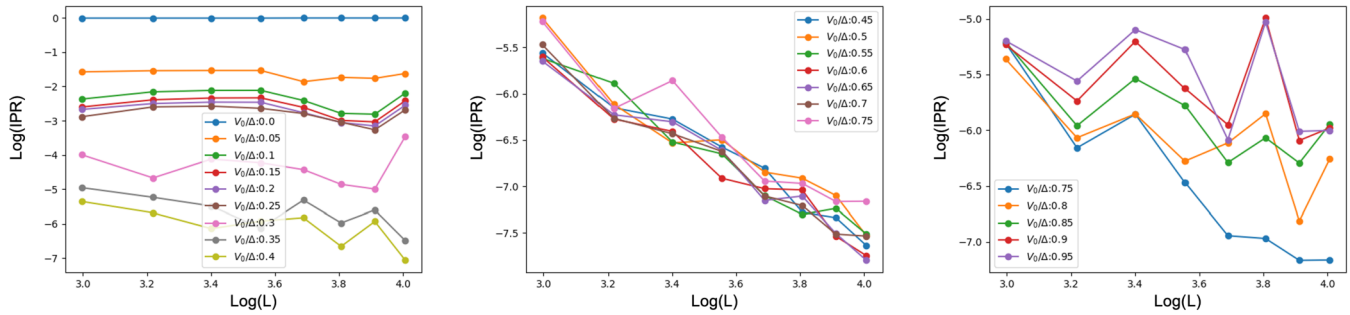

(a) (b) (c)

FIG. 17. IPR of the states that is in the middle of the spectrum. The x axis is Log(L) and the y axis is Log(IPR) for (a) small V_0, (b) intermediate V_0, and (c) large V_0.

We find that in both cases, IPR has a stronger system size dependence with increasing QP potential, which indicates that there are more extended states in $\vec{k}$ space. Moreover, we fit the dependence of Log(IPR) to the logarithm of linear system size L and find a linear dependence, $\text{Log(IPR)} = z\text{Log}(L) + b$. The trivial model has a slope $z \approx -1.88$, while for the nontrivial model $z \approx -1.37$. The slope of the trivial model is closer to the ideal scaling $z = 2$, which indicates that there are more localized states in real space in the trivial model than in the nontrivial model with large QP potential.

We further consider a nonuniform Berry curvature in $\vec{k}$ space with $B(\vec{k}) = B_0 + B_1 \sum_{j=1}^{3} \cos(\vec{k} \cdot \vec{b}_j)$, where B_0 is the uniform part as considered before. The B_1 term acts as a QP hopping term. We calculate the IPR with trivial and nontrivial B_0 and increasing B_1 (Fig. 14). For the trivial case, we find $z \approx -1.92$. For the nontrivial case, at small value of B_1, $z \approx -1.77$ and z decreases with increasing B_1. $z \approx 1.12$ within $2 \leqslant B_1 \leqslant 4$. The above results indicate that in the presence of nonuniform Berry curvature, there are more nonlocalized states (extended or critical) in real space in the nontrivial model compared to the trivial model (Fig. 15).

2. IPR of the two band model

We consider the Hamiltonian in Eq. (20). We let $V_1 = \Delta = 1$ and change V_0. The IPR's for various V_0 are shown in Fig. 16. We find that the slope of the Log(IPR)-Log(L) curve goes from $z = 0$ to $z \approx -1.58$ when V_0 is increased from 0 to 1. At small V_0, there is a band gap in the middle of the spectrum. When $V_0/\Delta \gtrsim 0.2$, the gap closes and the IPR values in the middle of the spectrum get larger after the gap closes, which indicates that there are extended states in the middle of the spectrum and they get localized with increasing V_0. We study the IPR of the states that are in the middle of the spectrum (Fig. 17) and find that there is an intermediate regime of V_0 where the IPRs of the states can be fit to a power law dependence to the linear system size with a power $z \approx -1.97$. Thus, the states in the middle of the spectrum are indeed localized in real space.

[1] Y. Cao, V. Fatemi, S. Fang, K. Watanabe, T. Taniguchi, E. Kaxiras, and P. Jarillo-Herrero, Nature (London) **556**, 43 (2018).

[2] Y. Cao, V. Fatemi, A. Demir, S. Fang, S. L. Tomarken, J. Y. Luo, J. D. Sanchez-Yamagishi, K. Watanabe, T. Taniguchi, E. Kaxiras *et al.*, Nature (London) **556**, 80 (2018).

[3] G. Chen, A. L. Sharpe, E. J. Fox, Y.-H. Zhang, S. Wang, L. Jiang, B. Lyu, H. Li, K. Watanabe, T. Taniguchi *et al.*, Nature (London) **579**, 56 (2020).

[4] C. Shen, Y. Chu, Q. Wu, N. Li, S. Wang, Y. Zhao, J. Tang, J. Liu, J. Tian, K. Watanabe, T. Taniguchi, R. Yang, Z. Y. Meng, D. Shi, O. V. Yazyev, and G. Zhang, Nat. Phys. **16**, 520 (2020).

[5] S. Chen, M. He, Y.-H. Zhang, V. Hsieh, Z. Fei, K. Watanabe, T. Taniguchi, D. H. Cobden, X. Xu, C. R. Dean, and M. Yankowitz, Nat. Phys. (2020).

[6] Z. Zhang, Y. Wang, K. Watanabe, T. Taniguchi, K. Ueno, E. Tutuc, and B. J. LeRoy, Nat. Phys. **16**, 1093 (2020).

[7] A. L. Sharpe, E. J. Fox, A. W. Barnard, J. Finney, K. Watanabe, T. Taniguchi, M. A. Kastner, and D. Goldhaber-Gordon, Science **365**, 605 (2019).

[8] M. Serlin, C. L. Tschirhart, H. Polshyn, Y. Zhang, J. Zhu, K. Watanabe, T. Taniguchi, L. Balents, and A. F. Young, Science **367**, 900 (2020).

[9] N. Bultinck, S. Chatterjee, and M. P. Zaletel, Phys. Rev. Lett. **124**, 166601 (2020).

[10] Y.-H. Zhang, D. Mao, and T. Senthil, Phys. Rev. Res. **1**, 033126 (2019).

[11] Y.-H. Zhang, D. Mao, Y. Cao, P. Jarillo-Herrero, and T. Senthil, Phys. Rev. B **99**, 075127 (2019).

[12] X. Lin and J. Ni, Phys. Rev. B **102**, 035441 (2020).

[13] X. Lin, K. Su, and J. Ni, 2D Mater. **8**, 025025 (2021).

[14] T. Cea, P. A. Pantaleón, and F. Guinea, Phys. Rev. B **102**, 155136 (2020).

[15] The incommensurability considered here should not be confused with the inherent incommensurability of the moiré pattern, which happens at a much smaller atomic scale and is irrelevant to the low energy physics we consider here.

[16] J. Sokoloff, Phys. Rep. **126**, 189 (1985).

[17] S. Aubry and G. André, Ann. Israel Phys. Soc. **3**, 18 (1980).

[18] T. Devakul and D. A. Huse, Phys. Rev. B **96**, 214201 (2017).

[19] J. H. Pixley, J. H. Wilson, D. A. Huse, and S. Gopalakrishnan, Phys. Rev. Lett. **120**, 207604 (2018).
[20] Y.-Z. Chou, Y. Fu, J. H. Wilson, E. J. König, and J. H. Pixley, Phys. Rev. B **101**, 235121 (2020).
[21] Y. Fu, E. J. König, J. H. Wilson, Y.-Z. Chou, and J. H. Pixley, npj Quantum Mater. **5**, 71 (2020).
[22] Y. Fu, J. H. Wilson, and J. H. Pixley, arXiv:2003.00027.
[23] C. Repellin and T. Senthil, Phys. Rev. Res. **2**, 023238 (2020).
[24] P. J. Ledwith, G. Tarnopolsky, E. Khalaf, and A. Vishwanath, Phys. Rev. Res. **2**, 023237 (2020).
[25] A. Abouelkomsan, Z. Liu, and E. J. Bergholtz, Phys. Rev. Lett. **124**, 106803 (2020).
[26] G. Roati, C. D'Errico, L. Fallani, M. Fattori, C. Fort, M. Zaccanti, G. Modugno, M. Modugno, and M. Inguscio, Nature (London) **453**, 895 (2008).
[27] B. Deissler, M. Zaccanti, G. Roati, C. D'Errico, M. Fattori, M. Modugno, G. Modugno, and M. Inguscio, Nat. Phys. **6**, 354 (2010).
[28] M. Schreiber, S. S. Hodgman, P. Bordia, H. P. Lüschen, M. H. Fischer, R. Vosk, E. Altman, U. Schneider, and I. Bloch, Science **349**, 842 (2015).
[29] P. Bordia, H. Lüschen, S. Scherg, S. Gopalakrishnan, M. Knap, U. Schneider, and I. Bloch, Phys. Rev. X **7**, 041047 (2017).
[30] J. Luck, Europhys. Lett. **24**, 359 (1993).
[31] J. Luck, J. Stat. Phys. **72**, 417 (1993).
[32] F. Iglói, J. Phys. A: Math. Gen. **21**, L911 (1988).
[33] P. J. D. Crowley, A. Chandran, and C. R. Laumann, Phys. Rev. Lett. **120**, 175702 (2018).
[34] P. J. D. Crowley, C. R. Laumann, and S. Gopalakrishnan, Phys. Rev. B **100**, 134206 (2019).
[35] U. Agrawal, S. Gopalakrishnan, and R. Vasseur, Nat. Commun. **11**, 1 (2020).
[36] J. Jung, A. M. DaSilva, A. H. MacDonald, and S. Adam, Nat. Commun. **6**, 6308 (2015).
[37] J. Jung, A. Raoux, Z. Qiao, and A. H. MacDonald, Phys. Rev. B **89**, 205414 (2014).
[38] H. C. Po, L. Zou, A. Vishwanath, and T. Senthil, Phys. Rev. X **8**, 031089 (2018).
[39] L. Zou, H. C. Po, A. Vishwanath, and T. Senthil, Phys. Rev. B **98**, 085435 (2018).
[40] H. C. Po, L. Zou, T. Senthil, and A. Vishwanath, Phys. Rev. B **99**, 195455 (2019).
[41] N. Marzari, A. A. Mostofi, J. R. Yates, I. Souza, and D. Vanderbilt, Rev. Mod. Phys. **84**, 1419 (2012).
[42] Y.-H. Zhang and T. Senthil, Phys. Rev. B **99**, 205150 (2019).
[43] M. Rossignolo and L. Dell'Anna, Phys. Rev. B **99**, 054211 (2019).
[44] B. Huang and W. V. Liu, Phys. Rev. B **100**, 144202 (2019).
[45] J. H. Han, D. J. Thouless, H. Hiramoto, and M. Kohmoto, Phys. Rev. B **50**, 11365 (1994).
[46] D. J. Thouless, Phys. Rev. B **28**, 4272 (1983).
[47] S. M. Girvin, A. H. MacDonald, and P. M. Platzman, Phys. Rev. B **33**, 2481 (1986).
[48] D. J. Thouless, M. Kohmoto, M. P. Nightingale, and M. den Nijs, Phys. Rev. Lett. **49**, 405 (1982).
[49] I. Dana, J. Y. Avron, and J. Zak, J. Phys. C **18**, L679 (2000).
[50] D. R. Hofstadter, Phys. Rev. B **14**, 2239 (1976).
[51] M. Onoda, Y. Avishai, and N. Nagaosa, Phys. Rev. Lett. **98**, 076802 (2007).
[52] E. Prodan, T. L. Hughes, and B. A. Bernevig, Phys. Rev. Lett. **105**, 115501 (2010).